EFFECTS OF ENVIRONMENTAL CONDITIONS ON ELECTRICAL CHARACTERISTICS OF PHOTOVOLTAIC MODULES AT UH MANOA: A MONITORING AND ASSESSMENT REPORT

A THESIS SUBMITTED TO THE GRADUATE DIVISION OF THE UNIVERSITY OF HAWAI‘I AT MĀNOA IN PARTIAL FULFILLMENT OF THE REQUIREMENTS FOR THE DEGREE OF

PROFESSIONAL MASTER OF GEOSCIENCE

IN

GEOLOGY AND GEOPHYSICS

JULY 2016

By

Ksenia Trifonova

Thesis Committee:

Janet Becker, Chairperson

Severine Busquet

Paul Wessel

Keywords: photovoltaic, monitoring, performance, weather

Abstract

This study comprises the monitoring and evaluation of the outdoor performance of two types of commercial photovoltaic (PV) modules in Hawaii over the year 2015. The PV technologies studied here are micromorph tandem (a-Si/µc-Si) and polycrystalline (c-Si) modules. The performance evaluation of the PV modules is carried out for meteorological observations, and an algorithm is applied to several environmental parameters related to the position of the sun compared to the PV module surface i.e. angle-of-incidence (AOI) and air mass (AM). The results present an assessment of the main solar and meteorological parameters and their impact on electrical PV performance as shown by empirical relationships. Spectral effects are investigated using the average photon energy (APE) index. Both daily and seasonal variability of the module performance is assessed. Daily changes are analyzed over a range of AOI. The environmental parameters are evaluated by their impact on the current-voltage (IV) curves and subsequently PV system performance. The key parameter to PV performance that is considered here is current performance (IP). The performance of a-Si/µc-Si modules appears to show higher sensitivity to several environmental parameters compared to c-Si.

List of Nomenclature

AM	air mass	a-Si/µc-Si	micromorph tandem
AOI	angle-of-incidence (°)	c-Si	polycrystalline silicon
APE	average photon energy (eV)	α	sun elevation angle (°)
AT	ambient temperature (°C)	θ	zenith angle (°)
CI	clearness index	η	cell/module electrical efficiency (%)
DB	direct beam irradiance (W/m²)	λ	wavelength (nm)
DF	diffuse irradiance (W/m²)		
G	global irradiance (W/m²)		
I	electric current (A)		
V	electric voltage (V)		
P	electrical power (W)		
PV	photovoltaic		
PR	performance ratio		
XTR	extraterrestrial energy (W/m²)		

Subscripts

MP	at maximum power
SC	short-circuit
OC	open-circuit
POA	in the plane-of-array
TOA	on top-of-the-atmosphere
ROC	at Real Operating Conditions
STC	at Standard Test Conditions (1 kW/m², 25°C MT, AM1.5)

Table of Contents

List of Figures

1. Introduction

The Hawaii Clean Energy Initiative (HCEI) has set the goal to become fully dependent upon renewable energy by 2045, proving the state's commitment to green energy development. Hawaii's abundant solar resource favors the development of solar energy as a suitable means to help achieve the HCEI's goal. The Hawaii Natural Energy Institute (HNEI) is positioned to contribute to Hawaii's renewable energy efforts. Hence, research and development of solar photovoltaic energy is being pursued in accordance with the commitments to the state's renewable energy goals. As part of the Green Holmes Hall Initiative (GHHI), an energy infrastructure project, HNEI is fostering the understanding of photovoltaic power deployment through a research project on PV system performance on top of Holmes Hall at the University of Hawai'i at Manoa, which was initiated in 2010. The PV energy exploration and testing for rooftop applications is aimed at evaluating the performance of PV modules under a range of environmental conditions. The assessment of environmental factors that reduce or enhance the amount of solar energy collected by a PV module and subsequently converted into electricity, illustrates how PV systems perform under real operating conditions (ROC) specific to Hawaii.

Commercial and residential use of solar photovoltaic technology has seen a steady increase in Hawaii, motivating the development of a better understanding of how we can exploit different PV technologies to optimize the energy yield. The way that PV modules function when they are tested in a laboratory environment does not reflect the true performance of modules when exposed to the natural environment. In addition, environmental conditions vary with location. This study focuses on characterizing two PV technologies in the Hawaiian environment to assess how environmental parameters affect different module technologies, primarily in terms of current performance. A comprehensive assessment of the basic solar physics shall help to determine critical parameters influencing PV system performance.

The method for evaluating the performance of a photovoltaic (PV) module is to compare the module performance against that provided by the manufacturer in the module's specifications under Standard Test Conditions (STC). This method uses the performance criteria called performance ratio (PR), which relates the module's operating efficiency (η_{ROC}) under ROC to the theoretical output (η_{STC}) indicated in the manufacturer's specifications evaluated at STC, where $PR = \eta_{ROC} \div \eta_{STC}$ (Pierro et al., 2015). The ratio of actual to predicted power is estimated anywhere between 75% to 95% in the literature depending on PV system technologies and locations and has grown from less than 70% in the nineties to an average range

between 80% and 90% observed in most PV systems today (Nordmann et al., 2014). These quoted PR values include a conversion loss (~5%) from direct to alternating current due to wiring individual modules in the PV system (AC PR), hence the DC PR values are nowadays around 84-95%. In the following, we focus on DC PR. Under ROC, operating temperature, solar irradiance and the solar spectrum, for example, are subject to natural fluctuations that are not accounted for by STC resulting in lower system performance under ROC. The wide range of published PR values does not allow one to predict the actual performance of the PV system. Hence, this study's objective is to assess the weather conditions impacting the PR and to determine the average PR for Hawaii.

This present study describes the applied methodology for monitoring and testing of the PV modules and reports on their performance characteristics. The study begins with an assessment of the weather conditions at UH Manoa, understanding the variation that occurs daily and seasonally. Then the impact of environmental parameters on electrical PV performance is evaluated by assessing the current-voltage (IV) curve characteristics and PR based on the demonstrated empirical relationships. The report presents results that support empirical relationships between performance characteristics, while qualitatively assessing the impact of each parameter on module efficiency. Finally, the relationships among parameters are used in describing PV module efficiency under ROC for Hawaii.

2. Hardware

This study involves analyzing data to determine relationships among environmental parameters and PV performance that were recorded under the GHHI project on the roof of Holmes Hall, where two PV systems were commissioned at the end of 2010. This section introduces firstly the data acquisition system (DAS) selected and installed by HNEI in order to assess PV performance under given environmental conditions.

2.1. The PV systems

Two PV systems using two different PV technologies are operating on the roof of Holmes Hall. Figure 1 shows the micromorph tandem (a-Si/µc-Si) (Mitsubishi Heavy Industries (MHI) MT130, 130W) in the front row and the polycrystalline (c-Si) (Kyocera (KYO) KD205, 205W) in the back rows. The first PV system is comprised of a 3kW system made of 24 micromorph PV modules (MHI), which is a technology that combines a layer of amorphous silicon on top of a microcrystalline silicon cell (Keppner et al., 1999). The second system is rated at 5kW consisting of 26 polycrystalline PV modules (KYO). In both systems, the PV modules are connected in series and in parallel to a string inverter that converts the DC power of the PV modules into AC power and feeds it safely into the electrical grid. The PV modules are mounted on top of the flat roof and are tilted according to latitude with a 20° tilt to the horizontal plane and a 180° orientation towards true South. The PV systems were instrumented to record electrical performance and weather conditions. In 2015, a new instrumentation was used to investigate further the PV performance through collecting the electrical characteristics of individual PV modules. The following section describes the instrumentation used to monitor the weather conditions. The analysis uses the data collected by the IV tracer that is described thereafter.

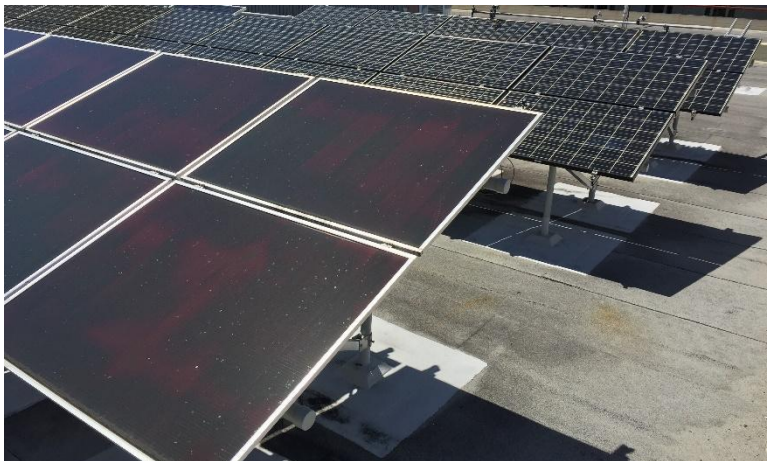

Figure 1 – Rooftop installation of the two tested PV technologies, micromorph tandem MHI (front) and polycrystalline KYO (back).

2.2. The monitoring equipment

The weather station system consists of different sensors that provide measurements of the solar resource and of the environmental conditions such as the ambient temperature, relative humidity, barometric pressure, wind speed and direction (Figure 2, top). A thermopile pyranometer (Hukseflux LP 02) (Figure 2, bottom right) and a masked pyranometer (Delta-T SPN 1) (Figure 2, bottom left) were selected to collect

information on the solar resource including global and diffuse irradiance, from which we calculate the direct beam irradiance. There are also cheaper solar sensors i.e. solar cell pyranometers surrounding the PV arrays also used in the following analysis. The results vary depending on the measuring instrument, with lower PR for data collected with the thermopile compared to the solar cell pyranometer, which is consistent with the findings of Reich et al., 2011. For this study, the analysis is based on data received by the thermopile pyranometer, as this sensor collects data over a full spectral range, while the solar cell spectral response is limited. All solar sensors are located in the plane-of-array (POA) to record the solar input received by the PV modules. This includes a spectroradiometer (Eko MS 700) that records spectral irradiance measurements, which refers to the energy distribution as a function of wavelength of emitted radiation from the light source. The spectroradiometer records spectral solar irradiance in the range 350 to 1050 nm every 15 seconds in the POA. The other analog instruments described above sample every second.

Each instrument has its own limitations in terms of accuracy and operating conditions, including limited spectral and directional ranges.

Figure 2 – Parts of the weather station (top), thermopile pyranometer (middle), masked pyranometer (bottom left), and spectroradiometer (bottom right).

2.3. The IV tracer

Part of the following PV performance analysis is conducted on individual PV modules that were extracted from the PV systems previously described. An IV-tracer (Daystar Multi-Tracer) is designed to collect the electrical characteristics or current-voltage (IV) curves of the PV modules. IV curves were recorded every minute. During the year 2015, two sets of PV modules were tested with the IV tracer. Four micro-amorphous and two polycrystalline PV modules were tested from February to June and a second set of modules was tested from June to November. This provides information on the temporal change of the PV

module performance over a year of operation and gives information on the performance distribution of the PV modules constituting the five-year old PV systems.

3. PV performance and parameters

The following sections describe the PV modules, their electric characteristics, the specifications provided by the manufacturers in the datasheet, and the criteria used to characterize their performance. We end this section by introducing the parameters found in the literature that influence the PV module performance.

3.1. Electrical characteristics

A photovoltaic module is composed of interconnected photovoltaic cells that convert sunlight directly into electricity. When a PV module receives solar radiation, photons are absorbed as light enters the cells, thereby freeing electrons and creating an electric current usable by an external load. The operational characteristics of a PV module, within an electrical circuit can be represented by a current-voltage (IV) curve, as shown in Figure 3. The IV curve shows the relationship between the current (I) flowing through and the voltage (V) across the electronic device. The operating point for a PV device varies from no load or short circuit condition I_{SC} to infinite load or open circuit condition V_{OC}. The product of current and voltage is power (P). The maximum power point for a module is the operating point of maximum power output (P_{MPP}) that varies with environmental conditions. The current and voltage at the maximum power point is represented by I_{MP} and V_{MP}, respectively.

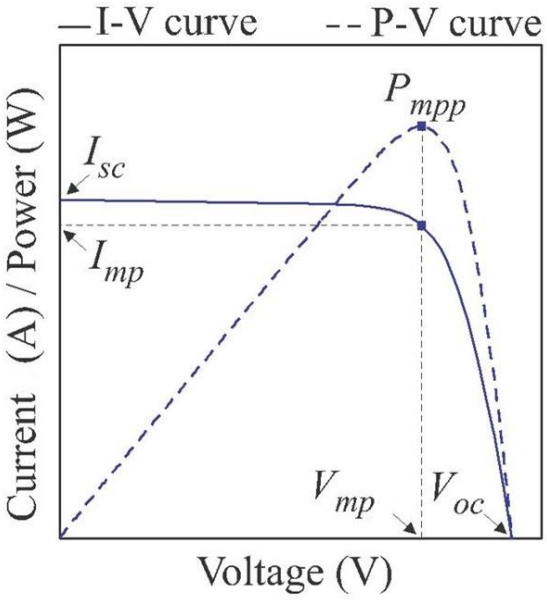

Figure 3 – Typical I-V curve of a PV module. (Coelho and Martins, 2012).

3.2. Performance characterization under Standard Test Conditions

Each PV cell and therefore each module is unique in terms of its electrical performance. Once assembled, the PV modules are evaluated by the manufacturer under a specified set of conditions, so as to ensure that each module is compliant within the specifications indicated in the datasheet. These so called flash tests are conducted in an indoor controlled environment under standard test conditions (STC). STC are defined by the ASTM standard G173-03, which includes a fixed cell temperature of 25°C and a solar irradiance in POA of 1 kW/m², whose spectrum corresponds to AM1.5G, the characteristic solar spectrum received on the US mainland. Table 1 shows the specifications for the polycrystalline (c-Si) module tested in this study. Table 1 provides the electrical characteristics under STC, as described in the previous section: P_{MAX} or P_{MPP}, V_{MP}, I_{MP}, V_{OC} and I_{SC}. The last two lines on the datasheet present the temperature coefficient for V_{OC} and I_{SC}, which result from testing at various cell temperatures. Those coefficients correspond to -0.35%/°C for the V_{OC} and +0.06%/°C for I_{SC}. For the micromorph modules (a-Si/µc-Si specifications in Appendix), the temperature coefficients are specified to -0.32%/°C for the V_{OC} and +0.06%/°C for I_{SC}. The a-Si/µc-Si PV module is less sensitive to variations in the temperature on the V_{OC}, which should correspond to less power loss at high operating temperature.

Table 1 – STC specifications indicated in the datasheet of the Kyocera c-Si PV module KD205GX-LP.

■ Specifications

■ Electrical Performance under Standard Test Conditions (*STC)	
Maximum Power (Pmax)	205W (+5%／−5%)
Maximum Power Voltage (Vmp)	26.6V
Maximum Power Current (Imp)	7.71A
Open Circuit Voltage (Voc)	33.2V
Short Circuit Current (Isc)	8.36A
Max System Voltage	600V
Temperature Coefficient of Voc	−0.120 V/℃
Temperature Coefficient of Isc	5.02×10^{-3} A/℃

*STC : Irradiance 1000W/m², AM1.5 spectrum, cell temperature 25℃

3.3. Performance criteria for outdoor testing

As mentioned in the introduction, the performance ratio (PR) describes the operating efficiency under ROC compared to the manufacturer‘s specifications at STC, relating the PV energy yield produced by the PV modules to the solar yield. The PR provides a means to compare PV systems of different sizes that receive different amounts of irradiation. The PV ratio is the PV energy normalized by the maximum power, P_{MPP}, achieved by the PV system divided by the normalized irradiation (Equation 1). The normalization in this document uses the STC specifications as indicated on the manufacturer’s datasheets.

The PV module performance was evaluated over the year 2015. In the following analysis, the performance is calculated daily, monthly and for the full period of testing. The PR is also calculated for shorter periods of time from 20 to 40 minutes in order to characterize the PV module performance at different times of the day, and consequently at different angle-of-incidence (AOI):

$$PR = \frac{Y_{PV}}{P_{MPP,STC}} \times \frac{G_{STC}}{Y_{SUN}} \quad (1)$$

with $Y_{PV} = \int_{\Delta t} P_{MPP} \cdot dt$ and $Y_{SUN} = \int_{\Delta t} G \cdot dt$

where Y_{PV} and Y_{SUN} the PV and solar yield during the specified time period, Δt, e.g. 20 minutes, 1 day; P_{MPP} the maximum power of the PV module; and G the irradiance collected in the POA.

PR accounts for the efficiency losses of the entire PV system when modules are wired together, as well as of the individual modules resulting from varying irradiance conditions, module temperature, spectral mismatch, recombination in the cells, reflection at the module surface and other effects such as soiling, shading and degradation. These loss mechanisms may also be studied through the current performance (IP) for the system and through the short-circuit current performance IP_{SC}, which has been shown to have the main impact on PR (Merten and Andreu, 1998; King et al., 2003; van Dam, 2013). The most significant controlling factor for I_{SC} is the irradiance G. To study the impact of other parameters, the current performance IP_{SC} is calculated similarly to PR using I_{SC} instead of P_{PV}, normalized by $I_{SC,STC}$ and divided by the normalized solar yield:

$$IP_{SC} = \frac{\int_{\Delta t} I_{SC}\ dt}{I_{SC,STC}} \times \frac{G_{STC}}{\int_{\Delta t} G_{POA}\ dt} \quad (2)$$

The most important loss mechanisms that affect IP_{SC} include the reflection and recombination losses, particularly at low irradiance levels and high AOI, and spectral and thermal effects. The reflection effect

describes the loss due to reflected light beams on top of the PV module surface, which increases with increasing incidence angle AOI (Okada et al., 2003). The recombination loss relates to electrons that recombine instead of creating a current, which is the dominant loss mechanism under low irradiance levels. The thermal effect represents an increase in IP with increasing cell temperature as indicated by the temperature coefficient (+0.06%/°C) mentioned previously in section 3.2. Finally, the spectral effect describes the performance variation due to changes in the incident spectrum, leading to higher or lower mismatch with the spectral response of the PV module, further discussed in the following subsection 3.4.

For a grid-connected PV system, only the operating point at maximum power (as selected by the inverter maximum point tracker) is monitored. The current performance IP is defined in (3) and the normalized voltage VN described in (4), dividing the operating voltage averaged for the period of analysis by the STC maximum point voltage of the PV system. The PR in this analysis is studied through IP and VN. PR values calculated using (5), were found very close to the product of IP and VN values for all periods of analysis including for the daily performance with differences below 0.5%.

$$IP_{SYS} = IP = \frac{\int_{\Delta t} I_{SYS}\ dt}{I_{SYS,STC}} \times \frac{G_{STC}}{\int_{\Delta t} G_{POA}\ dt} \quad (3)$$

$$VN_{SYS} = VN = \frac{\overline{V_{SYS}}}{V_{SYS,STC}} \quad (4)$$

$$PR_{SYS} = PR = \frac{\int_{\Delta t} I_{SYS} \times V_{SYS}\ dt}{P_{SYS,STC}} \times \frac{G_{STC}}{\int_{\Delta t} G_{POA}\ dt} \quad (5)$$

where $V_{SYS,STC}$ / $I_{SYS,STC}$ / $P_{SYS,STC}$ is the STC maximum power point voltage / current / power as specified in the datasheet combined with the number of PV modules in series / in parallel / in the system and V_{SYS} / I_{SYS} is the outdoor measurement of the PV system operating voltage / current.

The PV system location, including latitude, longitude and altitude, the PV systems set up, including tilt and orientation, as well as the environmental conditions impact the PV characteristics, such as light exposure and cell temperature, and ultimately operational performance. The analysis of the data shall aid at defining all critical parameters and their impact on the capabilities for electricity generation of a module with regard to the power performance and in particular, current performance.

3.4. Environmental parameters affecting PV performance

This section presents the main environmental parameters influencing PV performance and gives a brief literature review of each. The power of a PV module is proportional to the total irradiance received by a module in the plane-of-array (POA), termed global irradiance (G). G may be decomposed into its components, the direct beam (DB) and diffuse (DF) irradiance (Figure 4), which vary differently depending on the environmental conditions. Direct beam is the irradiance travelling in a straight line to the receiving surface of the module. Diffuse irradiance is the difference between global irradiance and direct beam irradiance, which is scattered crossing the atmosphere or reflected on surfaces including ground. The intensity of solar irradiance, its distribution between DB and DF, and the solar spectrum all are influenced by the angle-of-incidence (AOI), air mass (AM) and extraterrestrial radiation (XTR), illustrated in Figure 4 and discussed further in the study results.

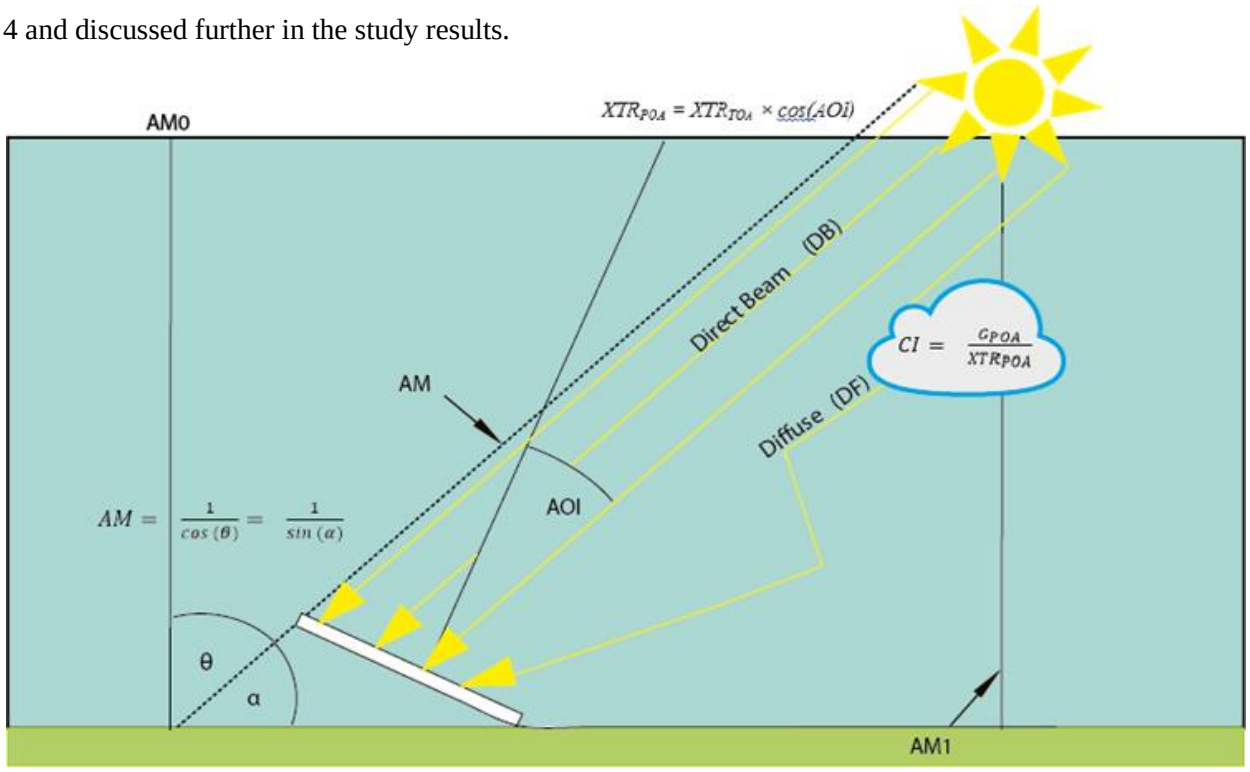

Figure 4 – Environmental parameters influencing solar yield in photovoltaic (PV) modules.

The solar irradiance received by the PV module surface, G or G_{POA}, depends on the solar irradiance available on top-of-the-atmosphere (TOA), XTR_{TOA}, minus the light absorbed by the atmosphere. The XTR received in POA, XTR_{POA}, depends on XTR_{TOA} and AOI, which is the angle between the direct Earth-Sun vector and the perpendicular line of the module surface:

$$XTR_{POA} = XTR_{TOA} \times cos(AOI) \quad (6)$$

Due to Earth's elliptical orbit, a seasonal variability exists in the distance between Earth and Sun and consequently in the amount of radiation received at the top of the atmosphere. Figure 5 shows the annual variation in XTR_{TOA} for the coordinates of the UH Manoa test location, corresponding to a yearly variation of only 100W/m². The annual average power density for XTR_{TOA} is approximately 1,366 kW/m² (Chen, 2011). As XTR_{TOA} varies only minimally, the greater impact on maximum solar radiation received by the PV modules in POA is due to the cos(AOI) factor in (6), which varies daily but also yearly as discussed in the results section.

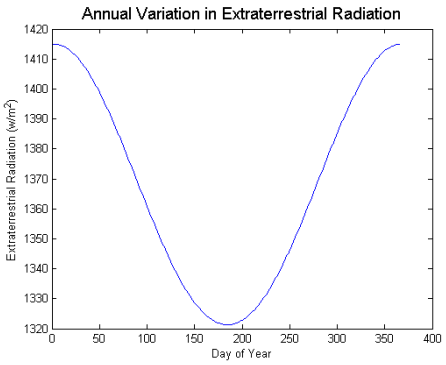

Figure 5 – Annual variation (blue line) of XTR_{TOA} for the coordinates of the UH Manoa test location.

Light travelling through the atmosphere is subject to absorption, scattering and reflection by cloud nuclei, airborne molecules, dust particles and gases such as carbon dioxide and ozone. The atmospheric conditions, particularly cloud cover, impact the spectrum, intensity and the distribution of direct beam to diffuse light. There are different ways to characterize the atmospheric conditions and this research studies the relationship between the indicators described below to understand which are most significantly impacting PV performance, if any.

An indicator that characterizes atmospheric conditions is the clearness index (CI), defined as:

$$CI = \frac{G_{POA}}{XTR_{POA}} \quad (7)$$

With increasing cloud cover as represented by decreasing CI, the spectral distribution across the wavelengths of the incident irradiance increases as a result of absorption by water vapor, which absorbs the long-wavelength range light with low energy content (Nakada et al., 2010).

The lower the sun is in the sky, the greater is the distance that light travels through the atmosphere while being exposed to these atmospheric effects. In PV studies, the calculated air mass (AM) coefficient represents a relative measurement for the length of the path that the sun's rays travel through the atmosphere to reach the module (Figure 4). AM is calculated from the horizontal plane at the altitude of the module and the zenith angle θ or the sun's elevation angle α, as $\theta + \alpha = 90°$:

$$AM = \frac{1}{cos(\theta)} = \frac{1}{sin(\alpha)} \quad (8)$$

AM is an important parameter for PV performance, because the solar spectral irradiance varies with different air mass conditions during the day and throughout the year (Nakada et al., 2010; Roumpakias et al., 2015). AM0 spectrum refers to the solar radiation available outside the atmosphere XTR_{TOA}. AM1 reflects the value for the thickness of the atmosphere that light needs to cross to reach a module at sea level when the sun is directly overhead (King et al., 2004). The STC AM1.5 corresponds to an elevation of arcsin(1/1.5) = 42°.

The solar spectrum describes the energy distribution of the incident light as a function of the wavelength. About 19% of solar radiation travelling through the atmosphere is absorbed by atmospheric gases (Litjens, 2013), and the gases absorb differently in varying wavelength ranges. Figure 6 describes the specific energy of the extraterrestrial irradiance (XTR_{TOA}) at AM0 and of the STC reference energy spectrum (AM1.5) for the irradiance received by a 37° tilted module surface. Figure 6 also distinguishes between the spectra of each irradiance component, the direct beam (DB) and the diffuse (DF) irradiance. All spectra show high energy content for wavelengths from 350 to 1050 nm, which is the STC wavelength range at AM1.5. The extraterrestrial and global irradiances, as well as DB are very similar in intensity and wavelength range. Global and direct irradiance are almost identical in the atmospheric absorption bands at different wavelengths, which are wavelength ranges in which radiation of certain frequencies is absorbed by different gases. The molecules with the highest absorption rates throughout the spectrum are water vapor (Litjens, 2013). At 630, 690, and 760 nm the absorption is mainly due to molecular oxygen, whereas at 1400 nm and higher carbon dioxide is the gas with the highest absorption rates. The diffuse irradiance of AM1.5G has lower energy and is shifted towards smaller average wavelengths.

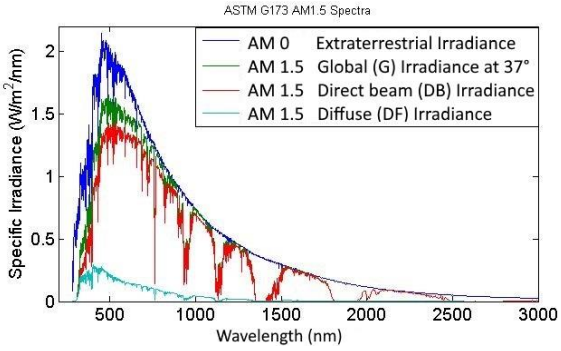

Figure 6 – ASTM reference spectrum at AM1.5 received by a 37° tilted module surface and XTR_{TOA} (Andrews, 2011).

The average photon energy (APE), measured in electron volts (eV), is related to the solar spectral content and refers to the distribution of photons across the wavelengths of the solar spectrum (Cornaro and Andreotti, 2013). This parameter indicates the energy content of light and influences electrical

characteristics of module performance as is discussed further in the results section. APE is a calculated value of the total energy in a spectrum divided by the number of photons, giving an average energy of all photons in the irradiance spectrum (Minemoto, 2009). APE is calculated using data collected by a spectroradiometer that measures the range of wavelengths across a spectrum. The spectroradiometer records spectral solar irradiance in a specific range of wavelength. APE values are sensitive to the wavelength range of the instrument. The APE of the STC spectrum using the spectroradiometer wavelength range of our instrument (350-1050 nm) is 1.88 eV (Minemoto, 2009). We will see later in the document that the APE can vary during the day and throughout the year, thereby giving us insights into the characteristics of the atmospheric conditions. Higher values of APE are observed with increasing cloud cover, while lower values of APE are observed with increasing AM, which has been found in other studies (Cornaro and Andreotti, 2012; Nakada et al., 2010). CI impacts the solar irradiance intensity and distribution between the DB and DF components, thereby affecting the solar spectrum due to scattering of light as it crosses the atmosphere. The average photon energy (APE) has been used by multiple laboratories since the nineties and was selected as an indicator for the solar spectral content to characterize the spectrum and to assess the impact of the solar spectrum on PV module performance.

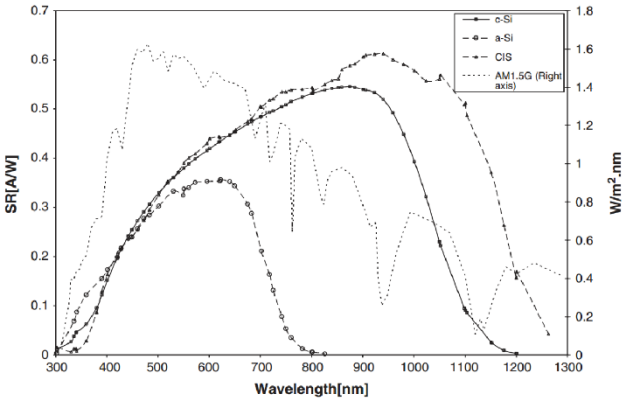

Figure 7 – Spectral energy density [W/m²×nm] (right y-axis) of the ASTM reference spectrum at AM1.5 and spectral response [A/W] (left y-axis) of different PV technologies (Silverman et al., 2014).

The portion of irradiance that a PV module can actually convert into current, depends on the incident spectrum of light and the spectral response of the PV modules. Figure 7 shows the spectral response of three PV technologies in comparison to the AM1.5G spectrum (van Dam, 2013). Again, as each module has its own performance, including spectral response, this graph shows the characteristic spectral range for different PV technologies. The polycrystalline c-Si PV modules have a wide range of absorption from 350-1050nm, whereby the amorphous a-Si PV modules have an absorption range between 300 to 780 nm. The micromorph tandem (MHI) is a dual cell combining the absorption range from two thin film cells. The top cell is an amorphous cell (a-Si) and the bottom cell is a microcrystalline cell (µc-Si 500-1000nm) whose combined range covers 300 to 1000 nm (Yamauchi et al., 2005). The last technology plotted in the graph is a thin film made of Copper indium gallium (di)selenide

(*CIGS*) with an absorption range from 350 to 1100 nm. The mismatch between a given solar spectrum and the spectrum at which a module operates results in a spectral loss. Although c-Si shows a wider wavelength range for its spectral response, it is at wavelengths where the incident energy content is small compared to a-Si, which operates in the most energy dense sections of the solar spectrum with higher photon flux density in the short-wavelength region compared to the spectrum at long-wavelength regions, which has a lower photon flux density (Nakada et al., 2010).

Figure 8 presents the variation of the main environmental parameters over the course of one day for two days in February 2015. The plots show the raw 1-second data, applying coefficients as indicated in the legend in order to visualize the parameters along the same range of values and to contrast the behavior for a day with clear sky conditions (left) and a day with overcast conditions (right). For a clear day, G looks like a bell curve and the DF component is minimal. APE spikes only at dawn and dusk, when the sun comes/goes over the horizon. For an overcast day, relative humidity is higher due to cloud cover, influencing solar intensity, distribution and spectrum, as more water vapor in the atmosphere causes more scattering of light. G is mainly made up of DF, both of which follow the trajectory of the CI, which is highly variable, thereby influencing the APE variability throughout the day and causing APE values to spike above values under clear sky conditions. Overall, we observe a higher APE, lower CI and higher DF for times of the day marked by overcast compared to clear sky conditions, indicating that cloud cover is a dominant factor influencing various environmental parameters.

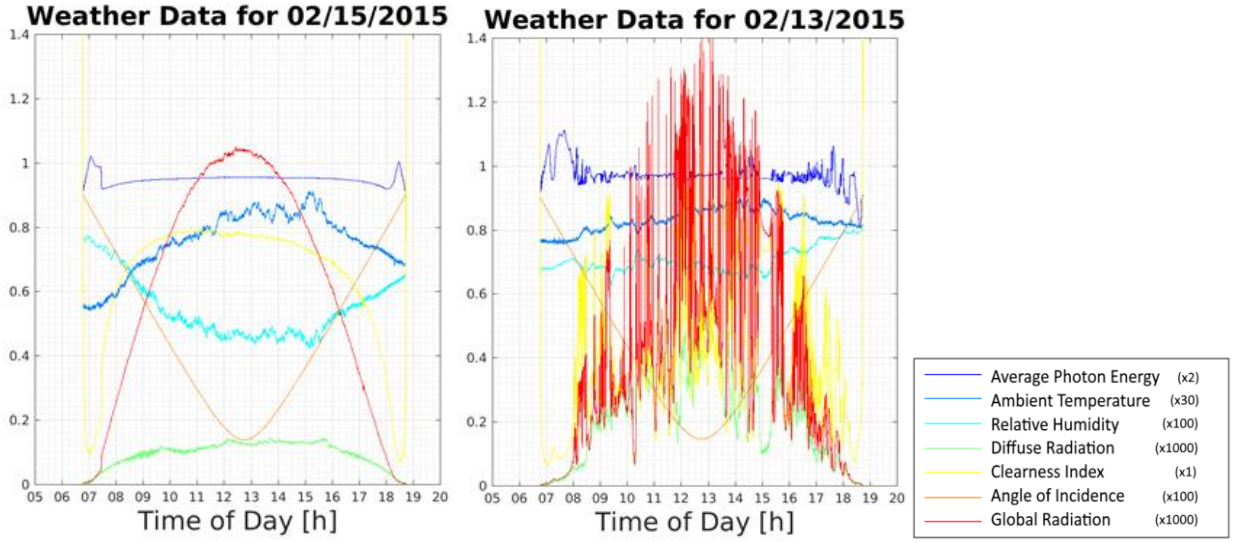

Figure 8 – Environmental parameters under different atmospheric conditions (left: clear sky, right: overcast) over the course of two days in February 2015.

4. Methodology

The analysis described here utilizes both collected data and computed parameters. The collected solar data consist of G and DF, from which DB is calculated. The weather conditions, including AT, and the IV-curves are likewise collected data. From the IV-tracer, we obtain the electrical measurements for individual module performance, including I_{SC}, V_{OC} and P_{MPP}, and from the HNEI DAS the data for the PV system performance, from which current performance (IP) and normalized voltage (VN) is calculated. In parallel to the logged data, the developed methodology includes the calculation of the parameters AM, AOI, CI and XTR. The SolPos algorithm developed at the National Renewable Energy Laboratory (NREL, Martin Rymes, 2000) applies astronomical equations to evaluate the position of the sun compared to a given location, date and time, and with the module setup, including orientation and tilt. APE is used as an indicator of the solar spectrum.

Due to the large amount of collected data and computed parameters (as illustrated in Figure 8), the analysis bins all data into angle-of-incidence ranges between 0° to 90° using 10°-bins, e.g. from 0° to 5°, 5° to 15°, until 85° to 90°, to assess the variability of the solar irradiance and other parameters over a day. We form 30 to 40 minute averages of the 1-second data and plot this data per AOI bin to visualize the daily variation of the parameters and to identify relationships and correlations among parameters during the day and throughout a year. To simplify the plots and whenever it helps visibility, we plot fewer AOI at 70°, 50° and 30° bins, including the daily averages and data for PV noon (defined below).

It is important to define the PV performance over a complete day of operation. The parameters are calculated per day as total daily average. The data used here is restricted to AOI below 70°, in order to limit error due to directional response of the solar sensors as well as to omit possibly biased data, as for instance the spikes in APE at dusk/dawn, mentioned in section 3.4.

The parameters are also estimated at PV noon, which represents a 20-minute interval around when the sun is closest to the normal to the POA of the PV surface. This value is representative of a midday performance when PV modules are expected to be most productive. Analyzing the time interval around where AOI values are at minimum proved to be informative for evaluating PV performance at maximum conditions in terms of irradiance and temperature. PV noon is equal to solar noon, when the azimuth equals 180°, or true South. In future work, the time interval of 20 minutes should be varied to consider the effects of the interval choice.

The daily results are averaged per month and year for 2015. The results are presented per AOI either versus time to visualize daily and seasonal variation or versus other parameters, to determine empirical relationships, particularly investigating the module behavior as a function of irradiance G_{POA}. Finally, we discuss the main parameters affecting IP (and thus PR) and their impact on PV performance.

5. Results

This section presents the study's assessment of the impact of environmental conditions at UH Manoa on PV performance. The first part on environmental conditions characterizes the local solar resource received in POA in terms of irradiation (or energy [in Wh/m²]) and in terms of irradiance (or power [in W/m²]), before studying the main indicators of atmospheric conditions. The second part of the results determines the average PV performance under ROC at the test site and defines the parameters that influence the daily and seasonal performance variation.

5.1. Environmental conditions

This section presents firstly, the local solar resource through irradiation and irradiance, G_{POA}, and provides a short analysis of the impact of PV orientation on the solar resource (XTR_{POA}). Secondly, we study the three indicators of the atmospheric conditions, namely CI, AM, and APE, and discuss the empirical relationships between the parameters. In the next two subsections, we refer to monthly and yearly values of the solar resource (Figure 9-12) and the environmental conditions included in Table 2.

5.1.1. Solar resource

For 2015, the GHHI test site received on average an irradiation in the POA of 5.8 kWh/m²/day with less than ⅓ from diffuse light and 72% (over ⅔) from the direct beam component. Figure 9 shows the yearly and monthly averages of the irradiation components collected at GHHI in 2015. We observe low seasonal variation at this test site, which can be explained by the high impact from cloud cover on monthly averages with no seasonal pattern in terms of cloud cover.

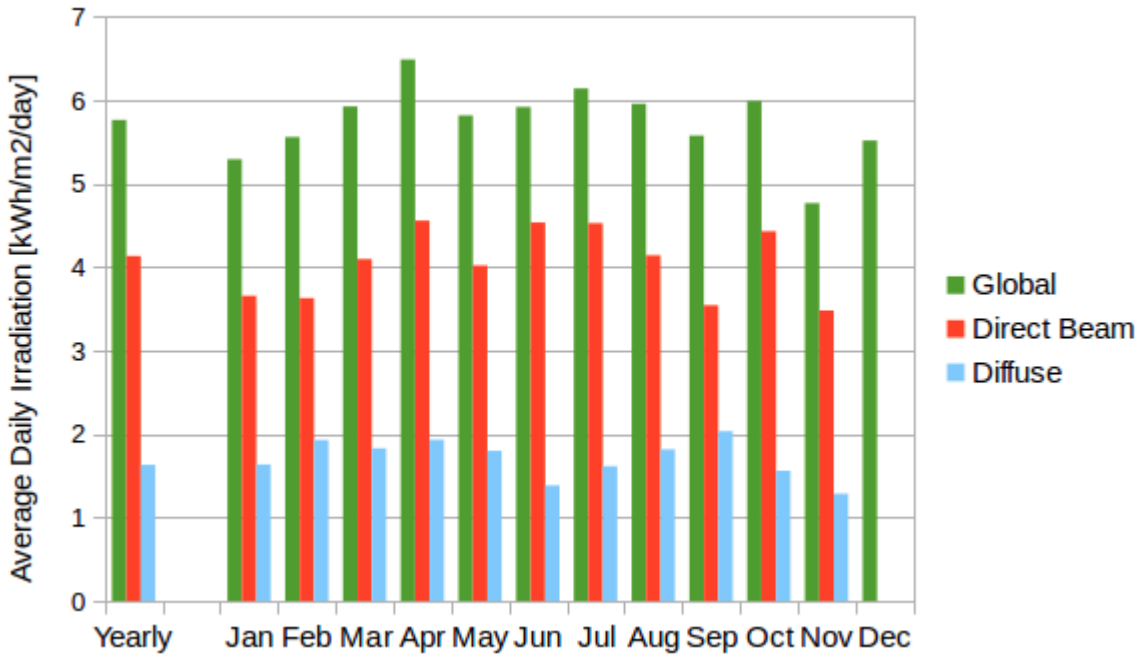

Figure 9 – Daily average irradiation received in the POA at GHHI in 2015 per month.

Figure 10 shows the annual variations for the solar irradiance, G, received in the POA per angle-of-incidence (AOI) over the year as measured by the solar cell (left) and by the pyranometer (right). The thermopile pyranometer measures the full solar spectrum whereas the solar cell (Apogee SP-110) has a limited operational range of 360 nm to 1120 nm, covering only part of the energetic spectral range. Thus the data chosen to describe the irradiance in this study is from the thermopile pyranometer. The thermopile pyranometer went through a period of calibration from July 15th to September 7th, showing noisy results over this period, which we removed from the data analysis. Hence, we also show the annual variation as measured by the solar cell, to visualize the seasonal variability over the entire year. The graphs show that G is relatively constant over time per AOI with the highest values observed at low AOI. At fixed AOI, G appears to be higher in the mornings than in the afternoons. Annual variation is visible in the peaks occurring at the vernal and autumnal equinoxes in March and September. This seasonal variation is related to the AOI reaching its lowest values at the equinoxes.

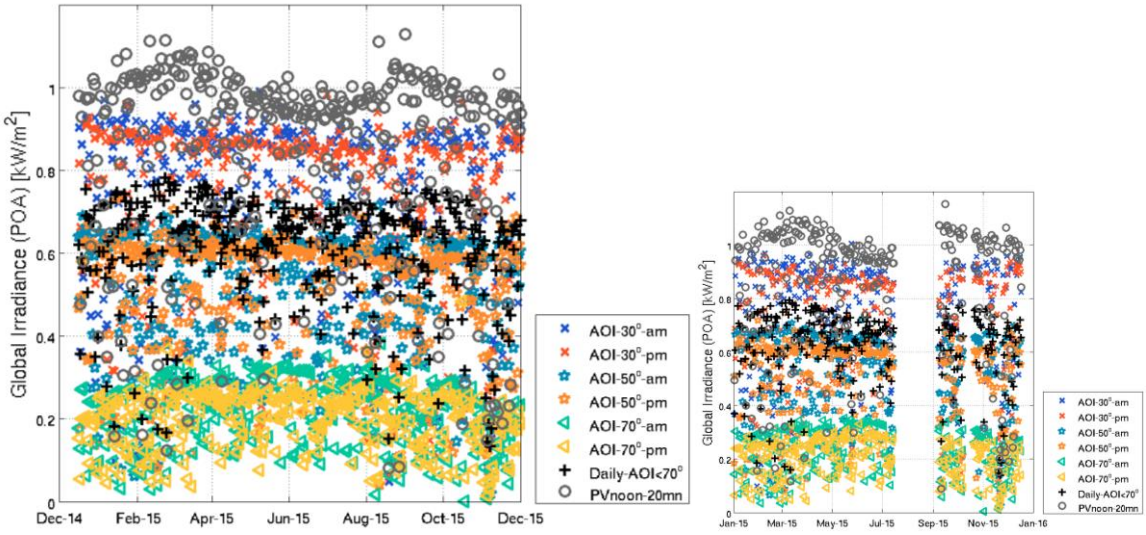

Figure 10 – Annual variation of solar irradiance G received in the POA per angle-of-incidence (AOI) for the year 2015 as measured by the solar cell (left) and by the pyranometer (right).

Another characteristic of the solar resource is a daily variation between the energy intensity in the morning (am) compared to the afternoon (pm). Figure 11 shows the difference of the solar energy collected per AOI in the morning compared to the afternoon, including the cumulative energy received from 0° AOI to 70°. This confirms that global irradiance G and direct beam DB are stronger in the morning at all values of AOI while more DF is collected in the afternoon. The cumulative energy (green line) indicates that most energy is collected at low AOI, with 80% of the daily energy collected for AOI below 45°.

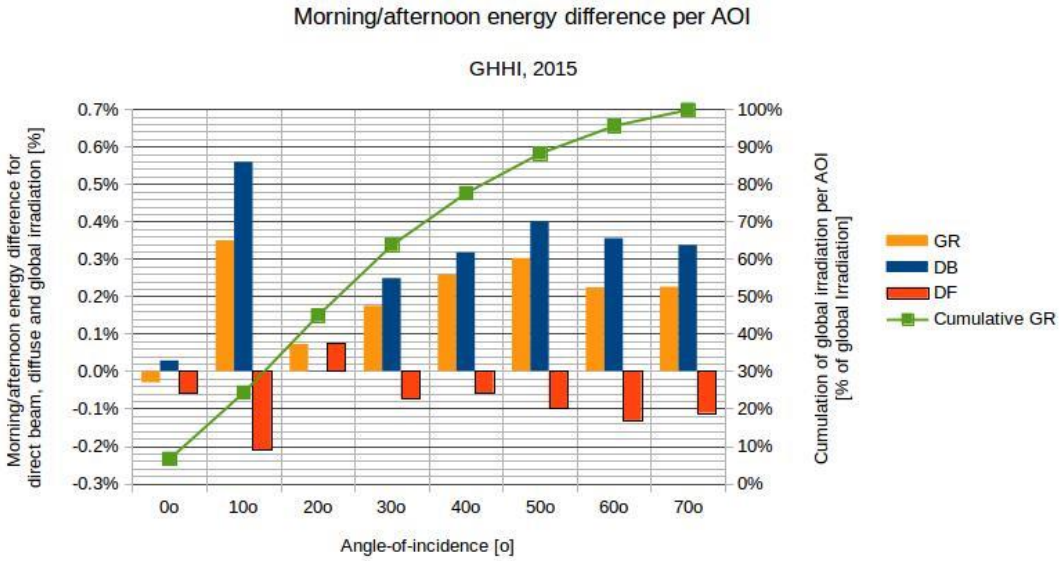

Figure 11 – Difference between solar energy received per AOI in mornings compared to afternoons and cumulative solar energy (green line) from 0° AOI to 70° in percent from yearly global energy.

The AOI depends on the location, including latitude, longitude and altitude, and on the orientation of the PV modules, including tilt and azimuth. Figure 12 illustrates the impact of the tilt (top) and azimuth (bottom) on XTR_{POA} (left) and minimum AOI (right) using the coordinates for Holmes Hall, demonstrating the variation in the availability of the solar resource on TOA received in the POA. XTR_{POA} varies with the seasons under varying tilt and azimuth, whereby tilt most impacts on the seasonal variation of XTR_{POA} and AOI at PV noon. For a 20° tilt as is the configuration for this study, solar radiation peaks during the vernal and autumnal equinoxes as shown in Figure 10, which is when AOI is lowest during the year. With decreasing tilt, the minimum AOI is lowest in summer, because the sun is the highest in the sky, leading to higher energy collection in summer compared to winter. Increasing the tilt shifts the seasonal variation of the solar energy yield and AOI leading to a higher solar energy yield in winter instead of summer for a tilt higher than 20°. The bottom panels (Figure 12) show the low impact of azimuth on the annual energy collection and AOI.

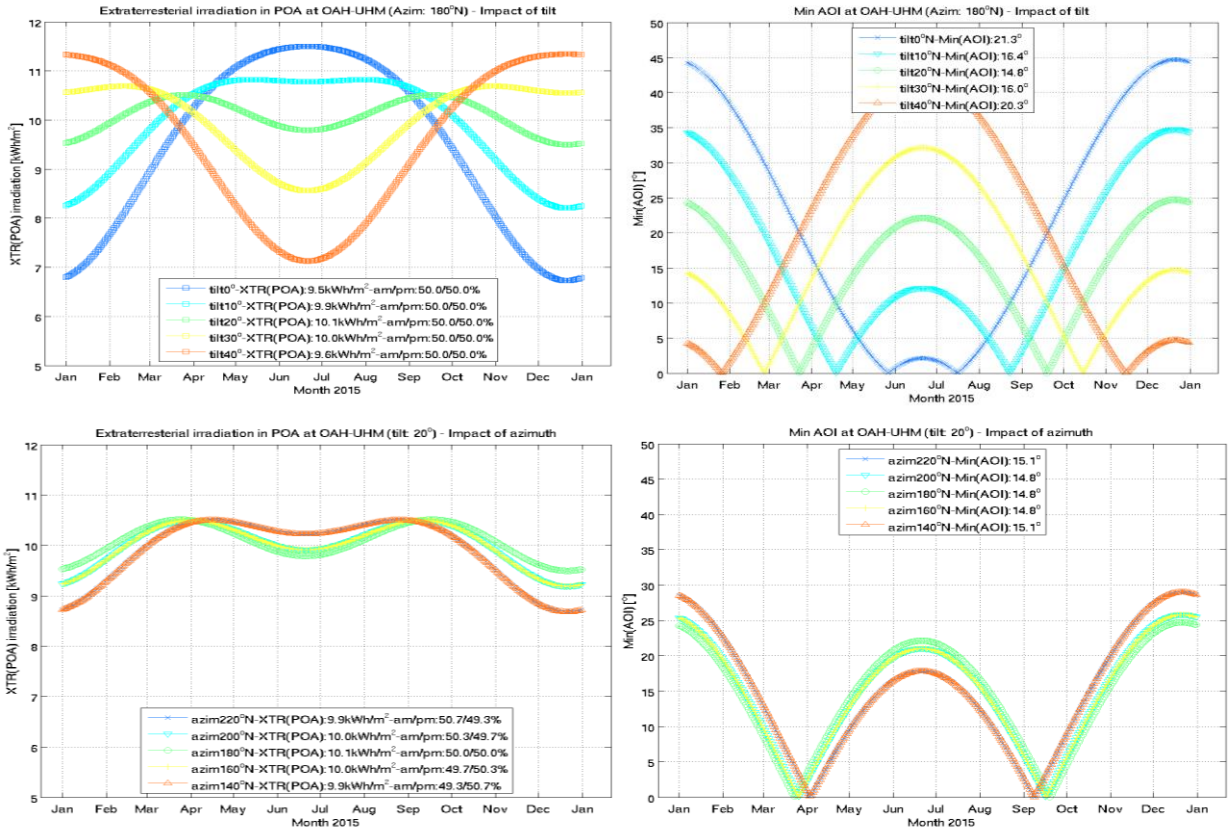

Figure 12 – Impact of tilt (top) and azimuth (bottom) on XTR_{POA} (left) and minimum AOI (right) for the test site location.

The total energy XTR_{POA} for the test site with the modules set at a tilt of 20° and an orientation towards true South (or 180° of North) is 10.1 kWh/m² per day. This values reflects the average solar energy per day based on the values for the year 2015. The cumulative impact of tilt or azimuth on the yearly energy received in POA (indicated in the legend of Figure 12) is minor. However, tilt and azimuth do show a small daily impact on solar energy collection with tilt showing the main impact on total daily energy yield. Changing the tilt from 20°, corresponding to the maximum energy collection for the test site, by ± 20° decreases the daily output by roughly 0.6 kWh/m². A 40° change in orientation from true South results in lower daily total daily XTR_{POA} of approximately 0.2 kWh/m². Changing the orientation from true South towards East or West also affects the amount of energy available in the morning or in the evening, respectively. The choice of configuration for the PV modules for this study provides relatively constant incident energy over the year.

5.1.2. Atmospheric attenuation

We now study the different indicators of the atmospheric conditions that influence the energy received at the modules: CI, AM, and APE. Table 2 shows the seasonal variation of the daily average values during 2015, by providing monthly averages and the annual average. The annual average CI is 0.59 and varies from 0.50 in November to 0.65 in April. Daily average APE vary slightly between 1.91 and 1.94eV with an annual average of 1.93eV, which is higher than the STC APE of 1.88eV. Daily average AM is the only indicator that shows significant seasonal variability with low values in summer and high values in winter, while APE and CI are influenced more by instantaneous daily cloud cover and show seasonal variations only in the peak values.

Table 2 – Annual and monthly average values for AM, CI, APE and AT.

	Yearly	**Jan**	**Feb**	**Mar**	**Apr**	**May**	**Jun**
AM	1.58	2.05	1.79	1.56	1.40	1.33	1.30
CI	0.59	0.57	0.57	0.59	0.65	0.61	0.64
APE	1.93			1.92	1.93	1.93	1.94
AT	26.50	24.50	25.12	23.96	25.82	25.47	27.49
		Jul	**Aug**	**Sep**	**Oct**	**Nov**	**Dec**
AM		1.31	1.37	1.49	1.71	1.99	2.14
CI		0.62	0.57	0.55	0.60	0.50	0.59
APE		1.94	1.94		1.92	1.93	1.91
AT		28.66	29.14	28.28	27.06	25.89	26.00

The indicator AM which represents the thickness of the atmosphere that solar radiation crosses varies with the time of day and well as the seasons (Table 2). Figure 13 shows the daily variation of AM as a function of AOI (left) and versus time (right) for the year 2015. AM ranges between 1.3 and 1.5 for AOI ranging from 20° to 30°. The daily average AM (black line) varies between 1.3 and 2.2 throughout the year. The seasonal variation of AM, however, increases with higher AOI. For the annual variability, higher values of AM are observed in the winter months than in the summer months, with values ranging from AM2.2 at AOI 70° in the summer and up to AM6 for the same AOI in the winter. This demonstrates a relationship between AM and AOI, where AM values and seasonal variation increase with increasing AOI, which depends on the location and orientation of the PV modules (Emziane and Altal, 2012).

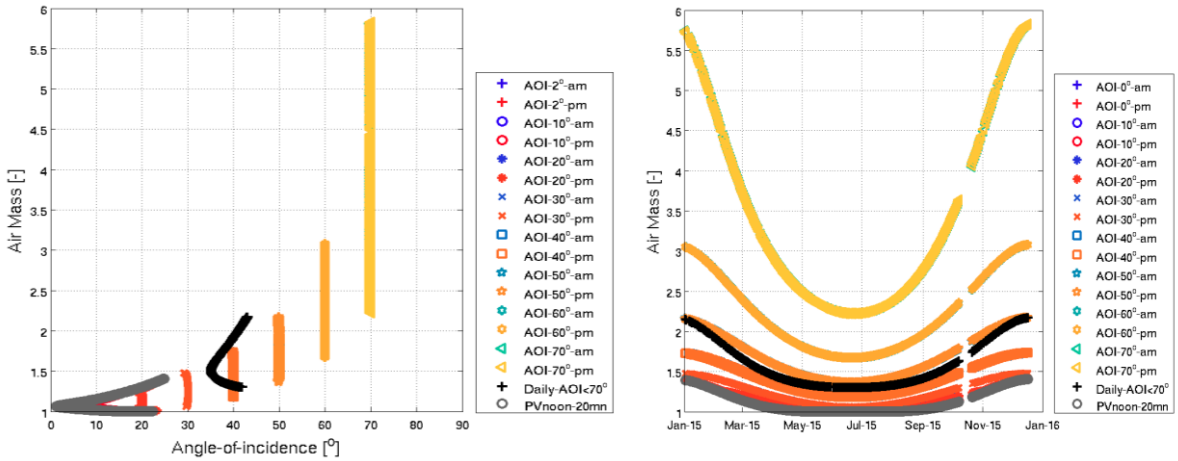

Figure 13 – Air mass AM as a function of all AOI (left) and versus time for the year 2015 (right) per AOI.

We next present the clearness index (CI) over the study period. Figure 14 shows CI per AOI versus time. The gap in the data from July 15th to September 7th is due to a break in the pyranometer monitoring as described in section 5.1.1. The maximum CI values, referred to as peak CI, occur at the lowest AOI around solar noon. Peak CI is mostly constant over time with a slight decrease observed in summer. Daily average CI (black crosses) typically vary between 0.6 and 0.75. Some months exhibit higher CI variability such as in January through March, September and November, impacting the monthly average values (Table 2). Below the peak CI, we observe CI values varying strongly due to cloud cover. Cloud cover refers to the conditions of the atmosphere, varying with the weather from clear sky conditions (high CI around 0.8) to increasingly overcast conditions (Figure 8). As cloud cover increases, more scattering affects the distribution of radiation by increasing the DF component while decreasing DB.

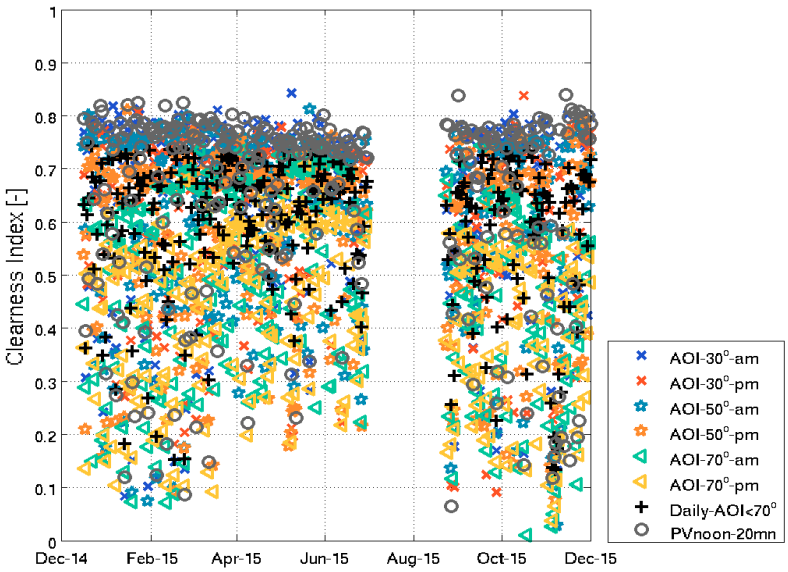

Figure 14 – Clearness index CI versus time per AOI for the year 2015.

Figure 15 shows the relationship between AM on CI (left) and CI at AOI 70° as a function of time (right). We observe a linear decrease of the largest CI values (peak CI) with increasing AM. We saw in Figure 13 the significant annual variation of AM which should also be observed for CI. We anticipate higher CI in summer while we observe a slight CI decrease at PV noon (Figure 14). Annual variation of CI is observed at high AOI with winter values for CI reaching as low as 0.5, and summer values of CI reaching 0.7 in the morning 0.6 in the afternoon. This observed difference between morning and afternoon CI is true at most AOI with an increasing am/pm difference for AOI above 40°.

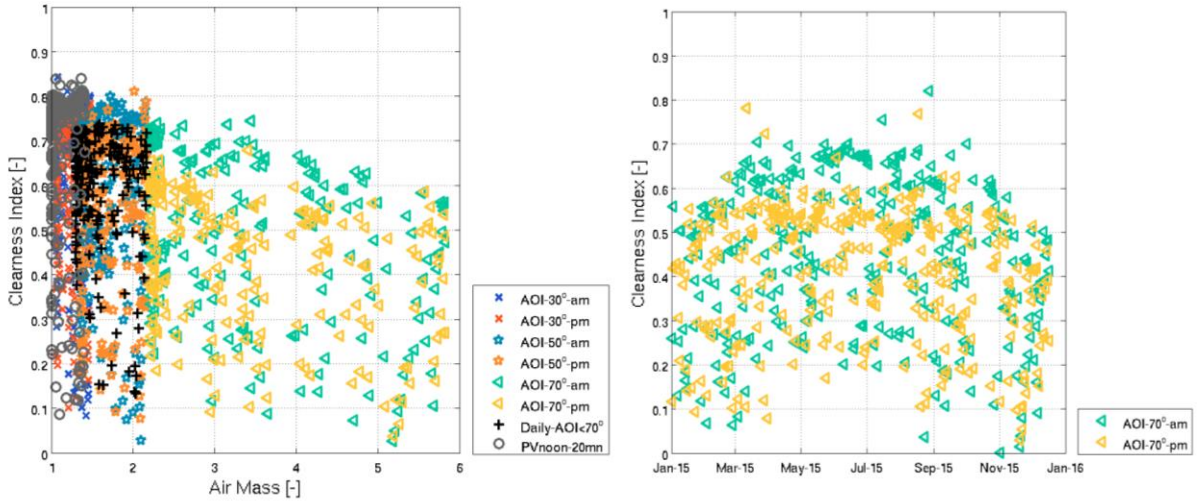

Figure 15 – Clearness index CI as a function of AM (left) and versus time for AOI 70° (right).

Higher CI observed in the morning than in the afternoon at high AOI and higher CI in winter than in summer could be related to the effects of ambient temperature (AT) on CI that show significant am/pm differences at fixed AOI. Figure 16 presents AT versus time at all AOI. AT appears lower at high AOI, particularly in the morning compared to the afternoon. We observe an increase in temperature from May to September, and another increase end of October, while the rest of the year AT is mostly constant below 28°C. Monthly average AT varies between 24°C in March and 29°C in September (Table 2) with an average of 26.5°C for the year 2015.

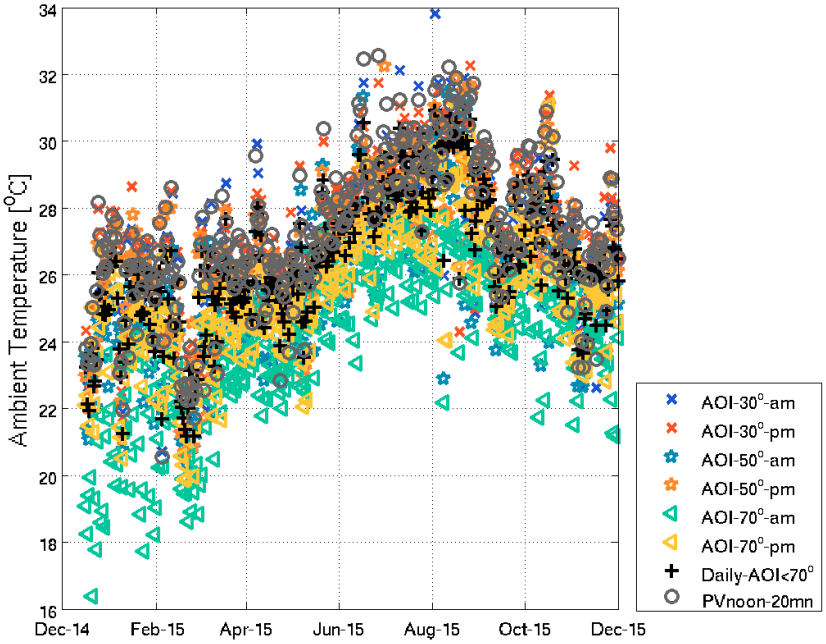

Figure 16 – Ambient temperature AT versus time per AOI for the year 2015.

Although the impact of AM on CI is apparent on both daily and seasonal time scales, the largest impact is at high AOI with less impact on the CI, both daily and at PV noon, which we suspect may be related to the AT. Cloud cover has a major effect on CI, which affects the distribution of DB and DF. As for the global irradiance G, the ranges of the DB and DF components increase with increasing solar resource received in the POA under decreasing AOI as shown in Figure 17, through plots of the DF irradiance as a function of AM (left) and the DB component as a function of CI (right). At high AOI (70°), DB and DF contribute approximately equal amounts to G, while DB becomes the main component of incident solar radiation received by the PV modules at low AOI, where it contributes roughly twice as much to total irradiance as DF. The right panel of Figure 17 shows that in the early morning for values of CI below ~0.3, the irradiance is purely DF until the sun rises over the horizon and DB becomes measurable. Above a CI value of ~0.3, a

quadratic increase in DB with increasing CI is observed, with a stronger increase in DB for decreasing AOI. DB is directly proportional to the extraterrestrial solar resource received in POA.

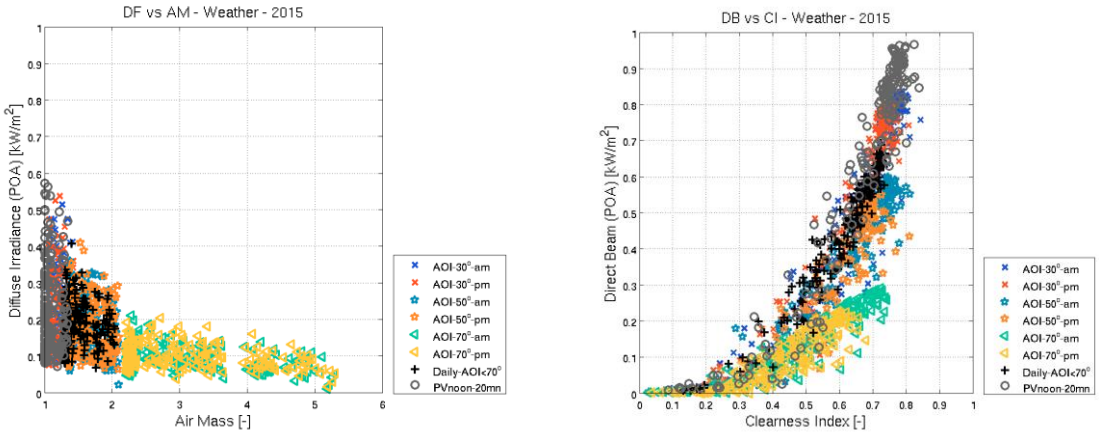

Figure 17 – Diffuse DF versus AM (left) and direct beam DB versus CI (right) under different AOI.

We next examine how the solar spectrum is described by the indicator APE. Figure 18 shows the annual variation of the average photon energy APE per AOI for the year 2015. The spectroradiometer was not operating continuously during the year due to updates that were conducted on the instrument. Therefore, APE values are missing for January, September, October and December. Daily average and PV noon APE vary over the year with highest values recorded in August and lowest in February. This tendency is not as clear in the monthly averages in APE (Table 2). For example, daily average APE in November is higher than in October. This is related to the cloud cover that significantly decreased the CI in November causing high variability in the APE values during that month. At all AOI, the measurements of APE are above the APE_{STC} (1.88eV), with the only exception at high AOI during winter. APE exhibits high variability at high AOI above 60° and seasonal variability with lower values in winter compared to summer.

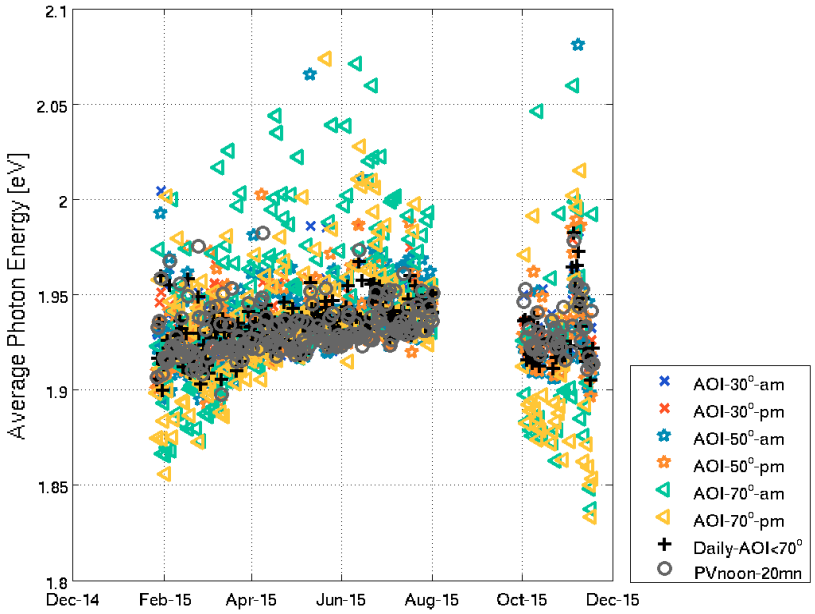

Figure 18 – Average photon energy APE [eV] per AOI versus time for the year 2015.

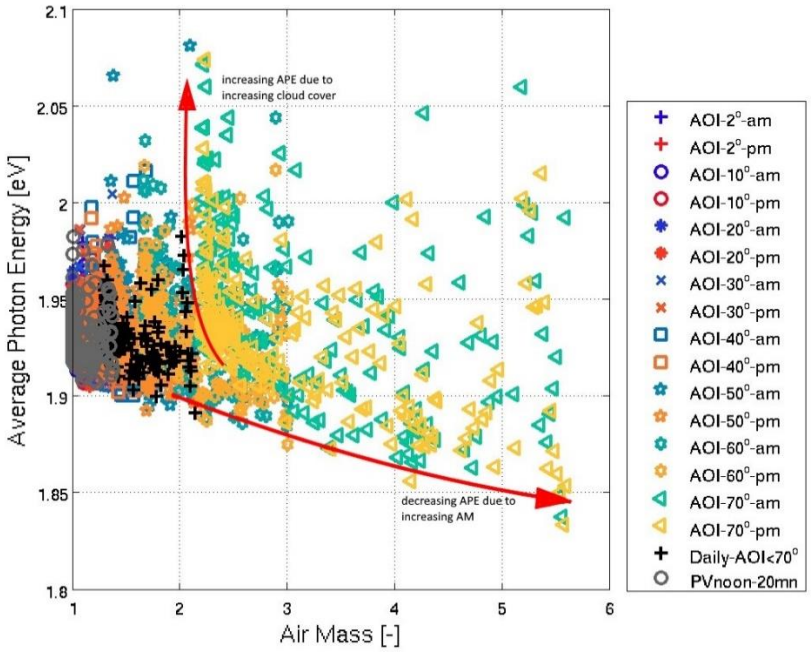

Figure 19 – APE for all AOI as a function of AM for the year 2015.

In summary, the APE exhibits higher values in summer than in winter and a seasonal variation at high AOI that is influenced by AM. Figure 19 shows the average photon energy (APE) as a function of AM. We

observe low values of APE decreasing with increasing AM. APE values are clustered in the range between 1.91eV and 1.96eV with scattered readings of higher values up to 2.08eV distributed at all AOI.

Figure 20 presents APE versus CI for the full year with all AOI included (left) and APE versus CI exclusively for AOI between 0° to 40° (right), representing the time during which solar yield is the highest. A large range of APE values is observed at high AOI. At low AOI, APE varies mostly between 1.91eV for clear sky conditions (CI~0.8) and 1.96eV for overcast sky conditions (CI~0.3), indicating elevated APE values at lower CI. At CI values under ~0.3 at dawn and dusk, or when highly overcast, DF is the major component to irradiance. As DF is lies within the lower wavelength range in the spectrum, APE is higher (Figure 6), hence, providing empirical evidence for somewhat higher APE values for DF compared to DB irradiance. At peak CI at solar noon, APE decreases with increasing CI, which is consistent with the seasonal variation of both CI and APE. Lower CI in summer is responsible for more scattering and thus higher APE values (seasonal variation ~0.03-0.04eV), whereby APE increases by around 0.05-0.1eV with decreasing CI due to increasing cloud cover.

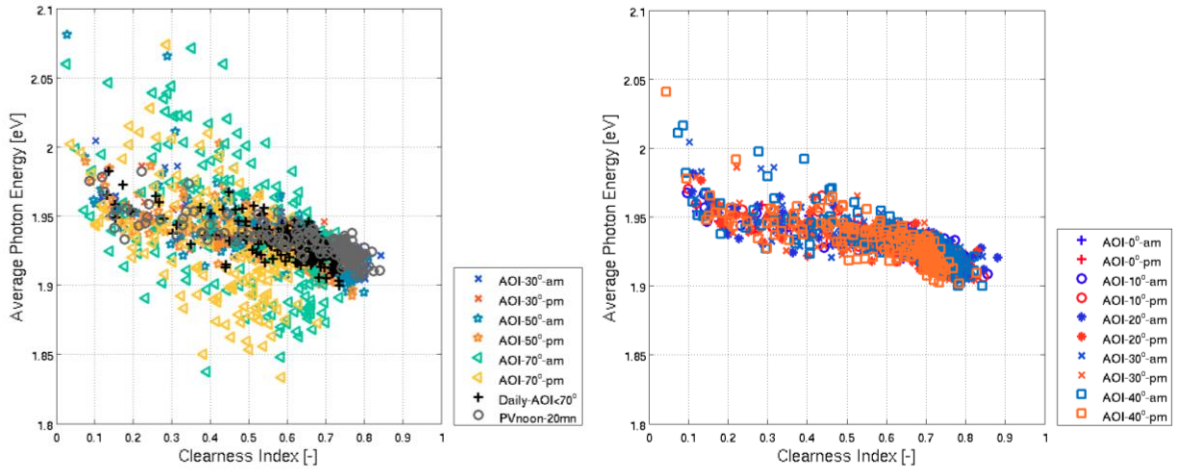

Figure 20 – Average photon energy APE as a function of CI for the full year with selected AOI included (left) and at AOI between 0°-40° (right).

When plotting APE versus DB for 2015 (Figure 21), a linear relationship is visible at PV noon between the two parameters. The plotted fitting curve (dashed blue line) is calculated using the least-squares method. In the regression, we remove the bottom 10% of the DB data, below 0.1kW/m², as the data at low irradiance is not representative of the linear trend. The impact of DB on APE at PV noon is estimated at -0.028eV per kW/m² with APE at 1.92eV when DB is 1kW/m². This variability of APE at all AOI is due to the effects of CI and AM.

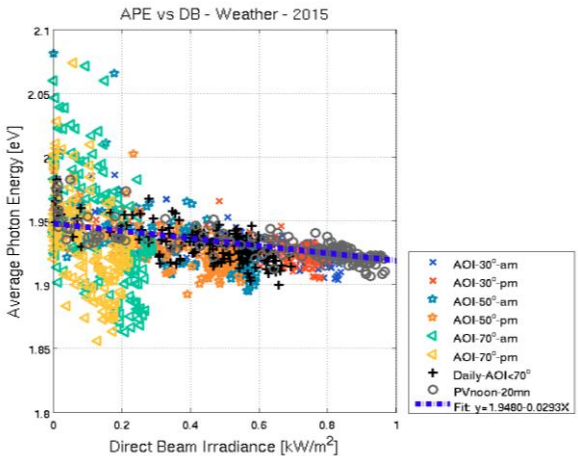

Figure 21 - APE per AOI as a function of DB irradiance for 2015.

In order to visualize the impact of AM on the solar spectrum, Figure 22 presents APE versus CI in June (average AM1.31 and CI of 0.62, left) and in November (average AM1.99 and CI of 0.5,right). In June, most APE values are recorded between 1.92eV and 1.96eV, decreasing with increasing CI. Higher APE values are recorded, however they are mostly limited to high AOI above 60°. In November, characterized by high AM as well as high cloud cover (CI~0.5), we also observe a linear relationship between APE and CI, where APE values are slightly lower at high CI than in June, but elevated at CI below 0.3. The impact of AM is apparent at high AOI leading to much lower values of APE than at PV noon due to a longer path of the sunlight travelling through the atmosphere.

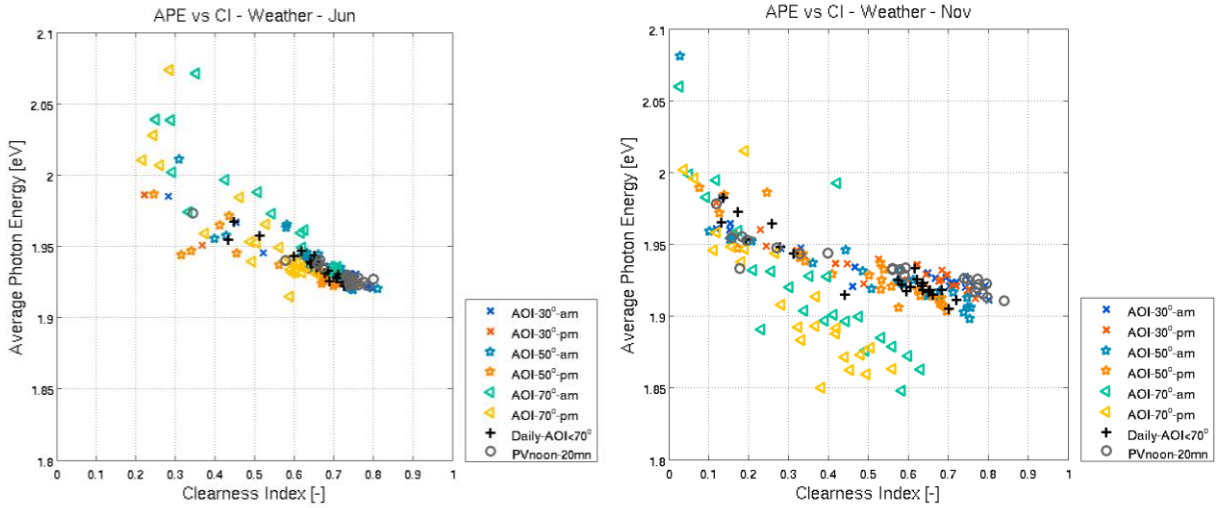

Figure 22 – Average photon energy APE per AOI as a function of CI in June (left) and in November (right).

From these observations, we conclude that APE has a significant relationship to CI but also is sensitive to AM at increasing AOI. Seasonal AM variability is visible at high AOI with low spectral energy recorded in winter. At low AOI, we observed a seasonal variation of APE with higher values in summer than in winter. In addition to the potential seasonal impact of AM, the APE annual variability could be attributed to the seasonal variation of CI and AM being lower in summer leading to more scattering and therefore

higher APE. On a daily timescale, CI increases with decreasing AOI leading to a decrease of APE, rapidly when CI falls below 0.3 with DF dominating the total irradiance, G, and then linearly with the contribution of DB to G increasing for CI above 0.3. This daily variation of APE has been observed in previous studies (King et al., 2004; Pierro et al., 2015) that find the incident spectrum to be more energetic in the short-wavelength range (higher APE) at sunrise and sunset than in the long-wavelength range (lower APE) at noon. The daily average APE values lie largely within the same range as the APE values at PV noon, indicating that the daily solar spectrum is dominated by the DB irradiance spectrum that has a narrower APE range than the DF component. Cloud cover impacts the daily variation of the CI, which in turn affects the distribution of solar irradiance across the spectrum. A high cloud cover increases the scattering of light, shifting the spectrum towards the short wavelength ranges, resulting in APE values higher than observed for clear sky conditions (clear sky APE ~1.91-1.92eV). AM impacts APE seasonally reducing low APE values collected at high AOI in winter by 0.06eV, but at the same time increasing the scatter between high and low APE values. Therefore we conclude that AM, CI and APE are all good indicators of the atmospheric conditions. Low values of CI are recorded at dawn/dusk or under overcast conditions, when DF is the dominant irradiance (Figure 17) leading to higher APE values. High CI corresponds to a high DB contribution to G leading to APE around 1.91eV. A thicker atmosphere crossed at high AOI in the winter compared to the summer affects APE values more significantly than CI. AM has a daily impact on CI, while for APE it affects the seasonal variation especially at high AOI.

This section presents the daily and seasonal variability of the main environmental parameters and indicators AM, CI, and APE under Hawaiian weather conditions for 2015. G is composed of the DB and DF components of irradiance, which are functions of the atmospheric conditions, particularly cloud cover. The results conclude on a daily time-scale, the variation in solar intensity and spectrum depends on the time of the day and weather conditions that both affect CI. As a result, we take CI as the most informative indicator of the attenuation of incident irradiance. CI is affected by both cloud cover and AM. The way that CI changes due cloud cover, is that for low CI values, G is mainly made up of DF, increasing APE, while for high CI values, G is mainly made up of DB, decreasing APE. The way that CI changes due to AM, on the other hand, is straightforward. The lower the sun is in the sky and the higher the AOI, the longer AM, thereby decreasing G, as the length of the path that light travels through the atmosphere impacts the amount of scattering and absorption. We have observed a clear relationship between APE varying with CI and AM, with CI lower in summer and higher in winter, and APE higher in summer and lower in winter.

Low CI corresponds to dawn/dusk or overcast conditions when the DF component of G is predominant leading to high spectral energy (APE). High CI is related to midday and clear sky conditions when DB is predominant inducing lower APE values. We observe seasonal variations in AM, CI, APE and somewhat AT and with the biannual cycle of the solar resources peaking at the two equinoxes and related to the PV location and orientation. AM impacts all others parameters by decreasing CI and APE when a thicker atmosphere is crossed during winter. The impact of AM on the parameters, however, occurs mostly at high AOI where the solar energy collection is minimal. The seasonal impact observed at PV noon when most solar energy is collected, is attributed to the lower observed values of CI and AM both leading to higher spectral energy (APE) in summer than in winter. The solar resource at UH Manoa is consistently high in intensity and energy all year.

5.2. Evaluation of PV performance under ROC

The PV module performance and parameters are described in section 3. Now, we examine how the variability in the environmental parameters affects the performance of both the individual PV modules as tested in the two PV sets over the first and second half of the year as well as the complete a-Si/µc-Si and c-Si grid-connected PV systems that were in operation over the year 2015. The PR is a function of the energy generated by the PV module or system divided by energy received by the PV module or system ($E_{PV} \div E_{SUN}$) which we use as the performance criteria for outdoor testing of PV systems under ROC. In this approach, the PR is considered as the product of the current performance (IP) of the system and the operating voltage normalized to STC (VN). The main daily variation observed for the PR is due to the variation in IP, while the impact of VN on the PR variation is considerably lower on a daily time-scale. In this study, we analyze the individual modules' short-circuit current performance IP_{SC}, which is compared to the systems' IP, reflecting the system's and module's abilities to absorb the solar resource and changing spectrum under ROC compared to STC.

The short-circuit current performance, IP_{SC}, reflects the part of solar radiation that can be usefully converted into an electric current (Pierro et al., 2015) and represents the main parameter of the PV module operation in the analysis of the individual PV module performance. Figure 23 shows the monthly average IP_{SC} for all tested PV modules during 2015. As mentioned previously, for each period of testing, February to June and June to November, six PV modules were tested including two polycrystalline (c-Si) and four micromorph tandem (a-Si/µc-Si). We observe higher IP_{SC} for all but one a-Si/µc-Si module compared to the c-Si modules. The a-Si/µc-Si PV modules show higher variability among the PV modules of the same

model, which is due to the performance distribution among newly installed modules and/or different degradation among modules. The variation in performance also is evident in June where the tested PV modules exhibit different performance. The IP_{SC} shows minor variability over the year, with a tendency to be slightly higher in summer than in December. When including all twelve tested modules, IP_{SC} averages 102.5% for a-Si/µc-Si and 98.4% for c-Si.

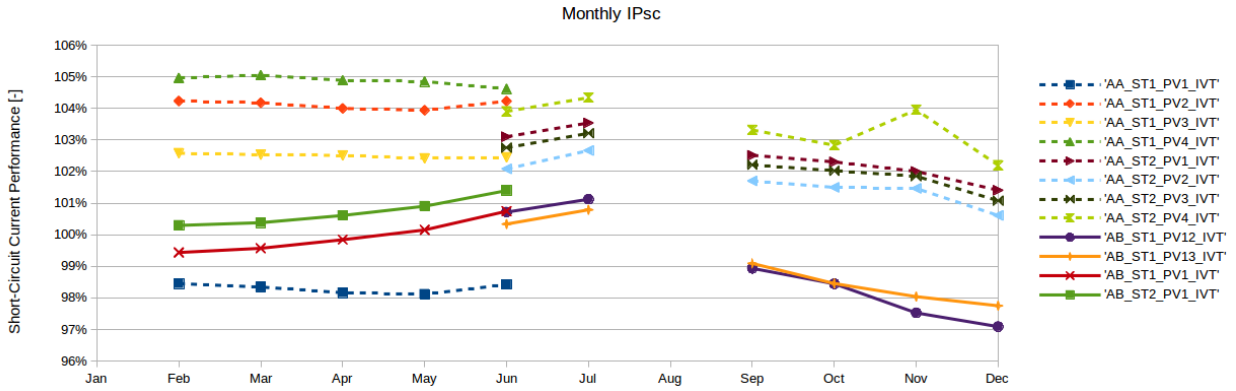

Figure 23 – Monthly average IP_{SC} versus time for multiple PV modules tested in 2015, a-Si/µc-Si (dotted line) and c-Si (continuous line).

Figure 24 shows the IP_{SC} at all AOI for two representative PV modules tested at different times of the year (left: February to June, right: June to December) for each PV technology (top row: a-Si/µc-Si, middle row: c-Si) as well as for the two PV systems (bottom row, left: a-Si/µc-Si, right: c-Si) over the entire year 2015. As previously mentioned, all tested PV modules have a fairly constant IP_{SC} at solar noon, slightly higher in summer than in winter. For all PV modules, there are periods of high variability, in February/March, in September and in November/December. These periods are attributed to low CI values, indicating high cloud cover and the associated large variability of the solar resource (Figure 12 and Table 2). In addition, all PV modules exhibit different performance at increasing AOI with significantly lower IP_{SC} values at high AOI in the mornings for the period of testing. The performance at AOI 70° also is found to be lower in the afternoon than at low AOI.

The IP_{SC} is the evaluation parameter for the individual modules, while for the PV systems, the appropriate evaluation parameter is the combined current performance at maximum power IP_{MP} of all PV modules in the system, IP_{SYS}. IP_{SC} shows a linear relationship with the current performance at maximum power point IP_{MP}, which determine the current performance of the whole PV system IP_{SYS}. When looking at the daily IP and IP at PV noon, the a-Si/µc-Si IP_{SYS} peaks in the summer, resembling the annual variation of APE, while

the variation in the c-Si IP_{SYS} is insignificant over the year, which may be partially explained by a potential temperature impact.

a-Si/µc-Si

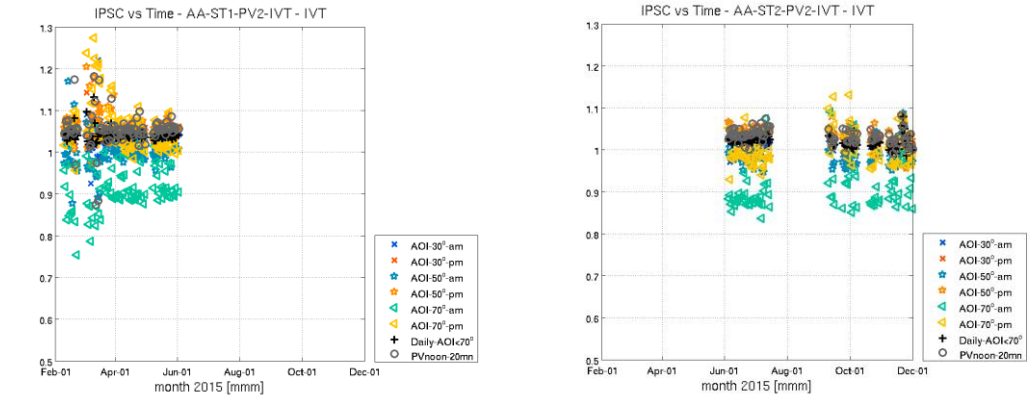

c-Si

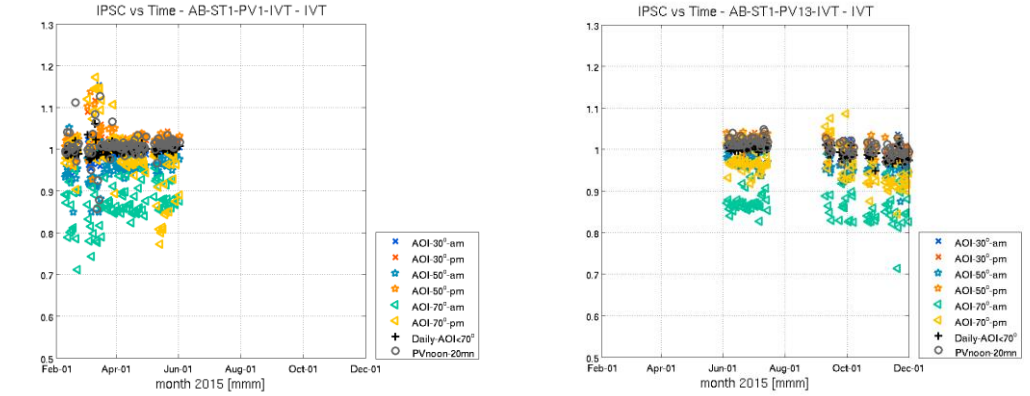

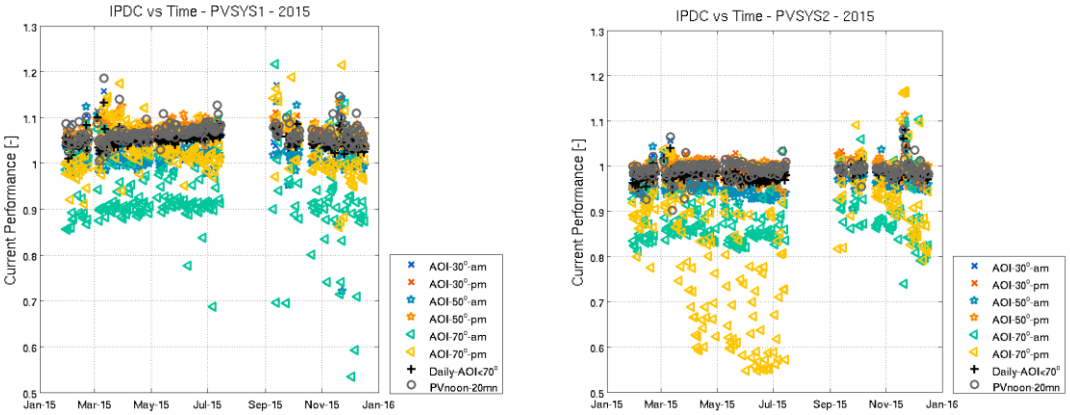

Figure 24 – IP_{SC} versus time for a-Si/µc-Si (top row) and c-Si (middle row) PV modules and IP of PV systems (bottom row, left: a-Si/µc-Si, right: c-Si). a-Si/µc-Si IP_{SYS} peaks in summer while c-Si is relatively constant over the year.

We next consider the effects of the main environmental parameters on IP_{SC} for all AOI, in order to fully visualize the relationships. Figure 25 present IP_{SC} versus G, DB, CI and APE for a single a-Si/µc-Si module operating during November 2015. We show in Section 5.2. that the aforementioned parameters are related. The results in Section 5.1. provide us with an assessment of the relevant parameters to characterize the PV module performance. Daily IP_{SC} (black crosses) decreases with increasing G, CI and DB. At high IP_{SC} under low irradiance conditions, when G is below 0.3 kW/m², we found that DB equals zero, CI is below 0.3 and APE above 1.95eV. When DF is the dominant component of G, IP_{SC} decreases with increasing G and CI, and decreasing APE above 1.95eV. For CI above ~0.3, APE is nearly constant which limits its impact on IP_{SC}. The most informative plots to analyze how environmental parameters impact gain and loss mechanisms of the solar resource are IP_{SC} versus CI, G and DB. We find that the variation of IP_{SC} with DB (Figure 25b) resembles the variation of IP_{SC} with G (Figure 25a), indicating the importance of DB in the generation of an electric current, both for daily averages and at PV noon. At high fixed AOI, IP_{SC} decreases with increasing G, DB and CI. At all AOI, the observed IP_{SC} is higher in the afternoon than in the morning.

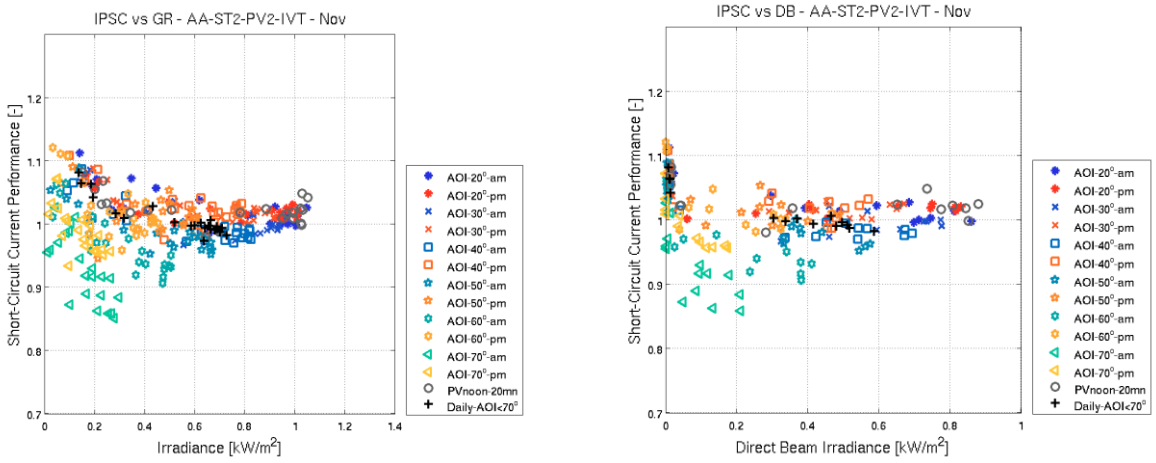

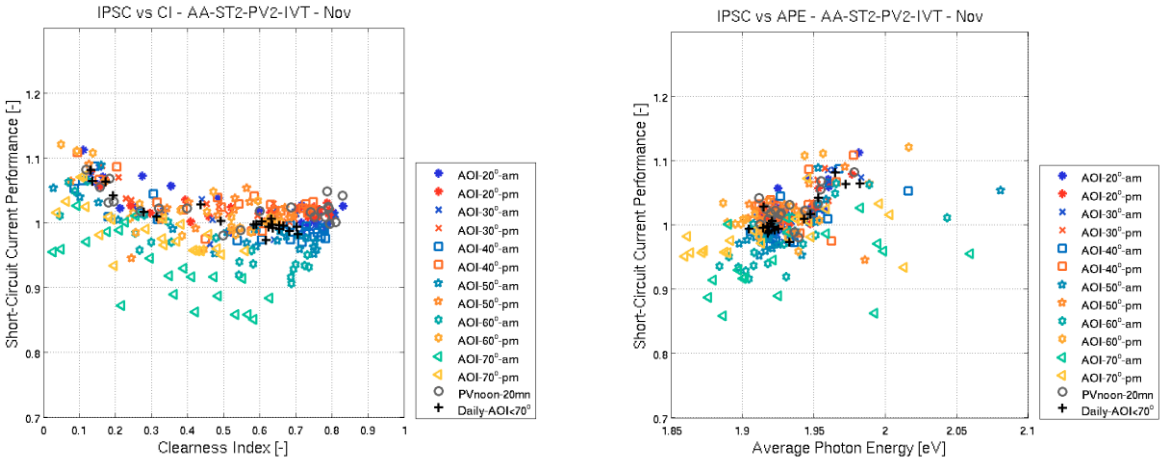

Figure 25 – IP_{SC} versus G (top left), DB (top right), CI (bottom left) and APE (bottom right) for all AOI for a single a-Si/µc-Si module operating over November 2015.

Figure 26 illustrates the impact of DB on the spectrum (APE) and CI for two months characterized by different AM. Figure 26 shows APE (top row) and CI (bottom row) as a function of DB at all AOI in June (left) and in November (right). We observe that for values of DB above ~0.1 at fixed AOI, the APE decreases linearly with increasing DB. In November, the monitored APE values are lower than in June at all AOI, but particularly at high AOI due to the high seasonal variation in AM. The seasonal CI variation is mostly visible at peak CI with higher CI in November than in June.

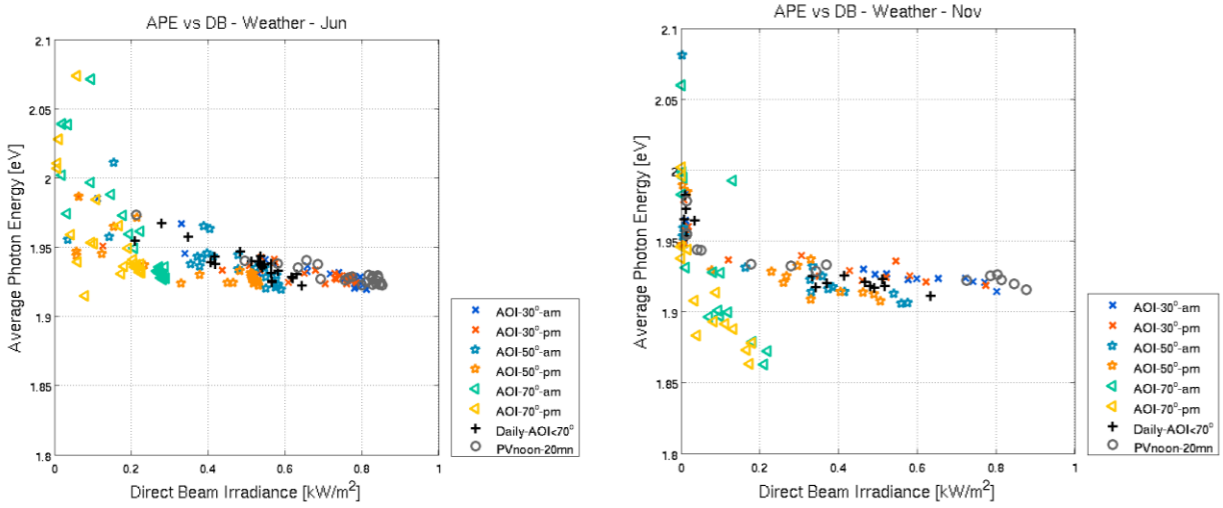

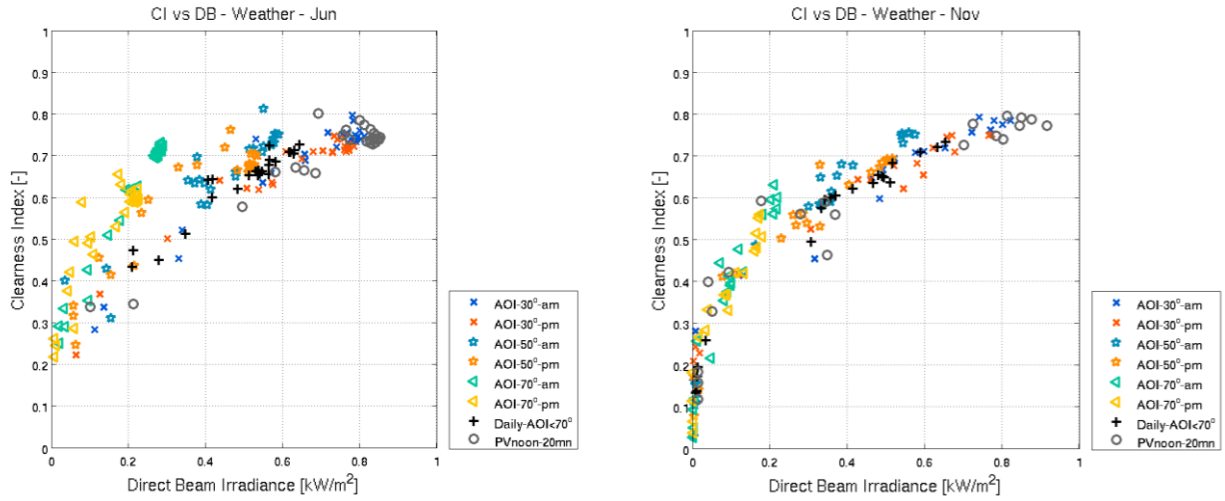

Figure 26 – APE (top row) and CI (bottom row) per AOI versus DB for the months of June (left) and November (right) 2015.

Figure 27 presents IP_{SC} versus DB for June (left) when the AM is low, and November (right) when AM is high. The top panel shows data for the a-Si/µc-Si module (MHI), the middle panels for the c-Si module (KYO). The bottom panels present the results for the IP of the two PV systems a-Si/µc-Si (left) and c-Si (right) versus DB for the complete year of operation.

For both PV module types, we observe higher performance in June than in November. This may be related to lower APE, higher CI or lower AT in November compared to June. Despite that slight drop in performance in November, the IP_{SC} versus DB curves are very similar between the two months and even between PV modules types. A slight difference exists at clear sky conditions (bottom data points with low IP, high DB) which may be due to different relationships among CI/DB/AT/AM depending upon the month of operation. For clear skies, IP increases with increasing DB and decreasing AOI. APE has a high seasonal impact at high AOI under clear sky conditions, which is not apparent in IP due to the low impact of seasonal APE on IP_{SC} at high AOI. Clear sky IP would therefore be affected mostly by recombination and reflection loss whose impacts increase at low G or high AOI. Morning performance is much lower than in the afternoon at all AOI which we also attribute to different CI/DB/AT/AM relationships depending upon the time of day. In the afternoons, IP_{SC} has high constant values at high DB with AOI above 50°. Afternoon IP_{SC} values decrease with increasing AOI above 50°, which is due to the PV modules being particularly affected by light reflection on the surface. For both PV systems, we plotted (not shown here) IP_{SYS} versus DB for the 2 selected months, June and November, as with the PV modules and observed similar results for IP compared to IP_{SC}. The bottom panels of Figure 27 represent data for the complete year of operation, showing higher

variability of the a-Si/µc-Si IP values, which is especially apparent at peak DB at PV noon as well as seasonally (Figure 24).

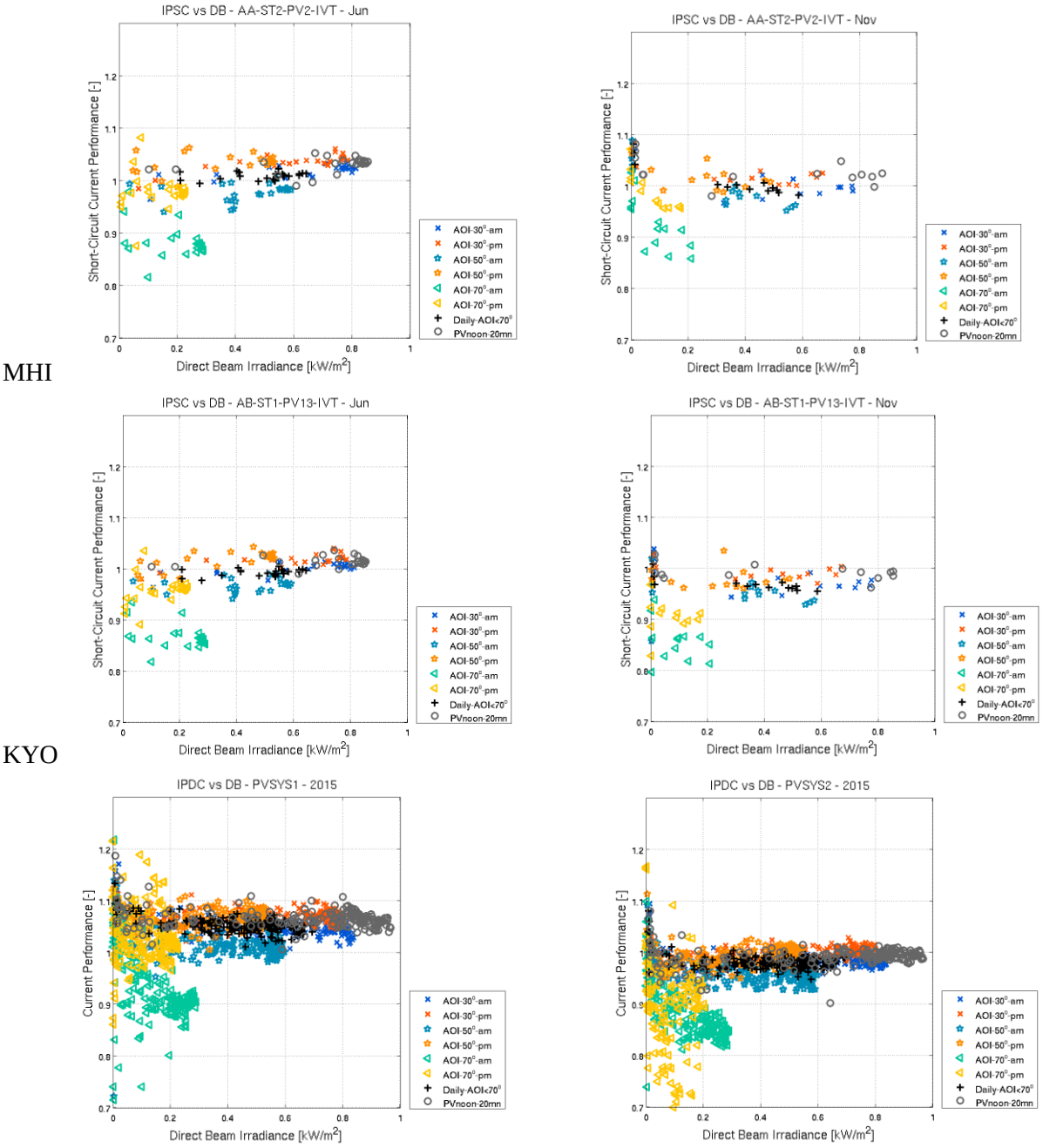

Figure 27 – IP_{SC} per AOI versus DB for a module of each technology (a-Si/µc-Si: top row; c-Si: middle row) for the months of June (left) and November (right). IP_{SYS} per AOI versus DB for both PV systems (bottom row, a-Si/µc-Si: left; c-Si: right) for 2015.

From Figure 27, we observe that for both months and both module technologies, DB shows a similar impact on IP_{SC}. The main impact on seasonal variation of IP_{SC} is attributed to CI, APE or AT. IP_{SC} is influenced by a daily APE variation when overcast conditions, described by low CI, promote scattering of light, changing the incident solar spectrum. No seasonal variation of IP_{SC} with APE is observed under clear sky conditions marked by high CI. The panels of Figure 27 aimed at demonstrating that the IP_{SC} for individual PV modules is representative of the IP for the PV systems, although additional losses due to operation at maximum power or due to system configuration and module mismatch may impact the IP_{SYS}.

Figure 28 presents IP_{SC} and IP_{SYS} per AOI versus CI for the two PV technologies. From this study, we are not able to distinguish the effects of the individual parameters (APE, AT, G/DB/DF) on IP_{SC} and IP_{SYS}, but we describe qualitatively the behavior of IP versus CI that will lead in the future to a better characterization of PV performance and the IP parameters. Firstly, the daily IP_{SC} is approximately constant at all CI for the c-Si module, while the a-Si/µc-Si IP_{SC} increases with decreasing CI showing enhanced performance at low CI below ~0.3. This is attributed to the higher sensitivity of the micromorph PV technology to shorter wavelengths and subsequently better performance under low G when DF is predominant (Pierro et al., 2015). This difference between PV technologies is not as apparent when considering the system's IP_{SYS}. More analysis is needed to understand the impact of combining PV modules on the current performance and the differences between the IP_{SC} and IP_{MP}. Secondly, plotting IP versus CI shows similar behavior to that observed versus DB (Figure 27). The irradiance G decreases with increasing AOI on clear days. Under clear sky conditions, CI decreases with increasing AOI and the relationship between CI and AOI or AM is different in the morning than in the afternoon (represented in Figure 28a by cooler and warmer colors), and also exhibits seasonal variability (represented in Figure 28a by grey circles at peak CI). The decrease in IP with increasing AOI is related to decreasing G. Both recombination and reflection losses are affected by G (section 3.3) and the losses increase with increasing AOI. Changes in IP with CI on clear sky depends of time of the day and of the year which we relate to variations in G/DB/DF, APE, and AT. More work is needed to differentiate the individual impact of those correlated parameters. Finally, we consider the behavior of IP with peak CI at PV noon, where we observe a decrease in IP with increasing CI that is larger in winter than in summer. The seasonal variation of IP at peak PV noon is attributed to the seasonal variation of APE and AT where APE decreases with increasing CI (Figure 22). When comparing the performance of the two PV technologies, a-Si/µc-Si shows higher variability than c-Si, which is particularly apparent for the PV system performance. This variation is clearly visible in the

variation of IP_{SYS} versus time in Figure 24. The difference in performance between systems and modules is possibly due to difference between IP_{SC} and IP_{SYS} and/or to the longer period of recording for the PV systems than for the PV modules. Higher seasonal impact on a-Si/µc-Si IP is related to the higher sensitivity of this technology to variations in the incident spectrum, compared to the c-Si technology.

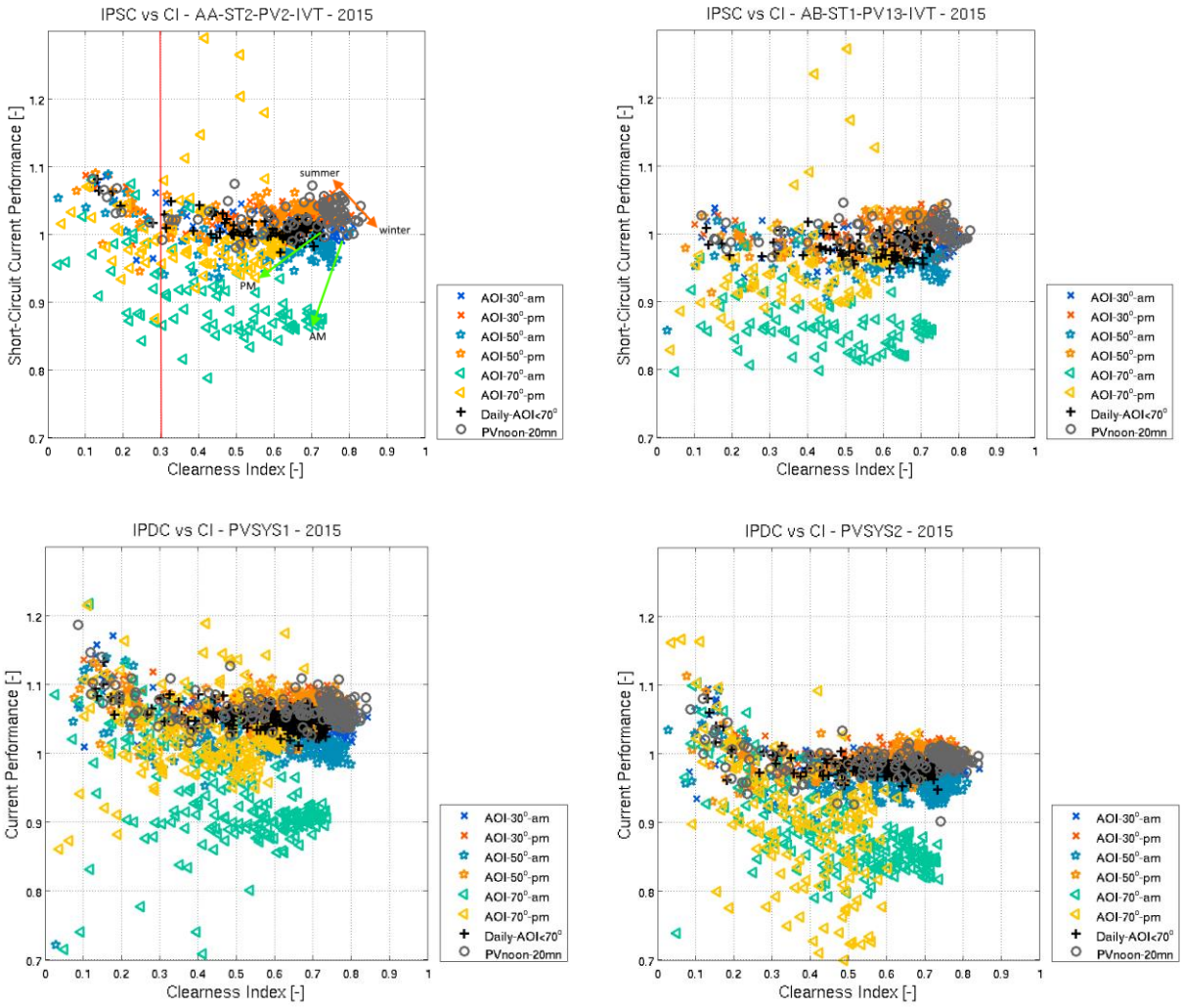

Figure 28 – IP_{SC} per AOI versus CI for a module of each technology (left: a-Si/µc-Si, right: c-Si) for full period of testing (June-November 2015) and IP_{SYS} for year 2015 on the PV systems.

The seasonal impact of peak CI on PV performance varies in opposition to the spectral energy as characterized by APE, and to a certain degree opposite to the ambient temperature, although AT is observed to peak in September rather than in summer. Both APE and AT increase in summer when sunlight has a

more direct path through the atmosphere. We also observe higher IP values for the a-Si/µc-Si module compared to the c-Si module, particularly in the summer, which is consistent with Ishii et al., 2013. This observation suggests that tandem a-Si/µc-Si modules are subject to a strong spectral effect represented by the APE, while c-Si modules are affected by the module temperature as suggested by Minemoto et al., 2009. A clear assessment of the effects of temperature, CI, G/DB/DF and APE on PV performance requires additional investigation.

In summary, IP_{SC} and IP_{SYS} as a function of G are presented in Figure 28 showing that the performance of the individual PV modules are comparable for the two PV technologies operating for the full year 2015. For clear sky conditions (bottom data points with low IP, high G), IP_{SC} increases with increasing G and AT, as well as decreasing reflection loss. At fixed AOI, IP_{SC} increases with decreasing CI, increasing DF and APE and decreasing reflection loss due to lower DB. IP_{SC} may be enhanced due to the high spectral energy of the diffuse irradiance at low G below ~0.4. Time of the day performance differences are likely due to a combined impact of lower AT, as well as lower APE and higher reflection loss due to higher DB in the morning than in the afternoon. Daily average IP_{SC} is slightly lower than at PV noon, which demonstrates the impact of the daily variation on the average performance.

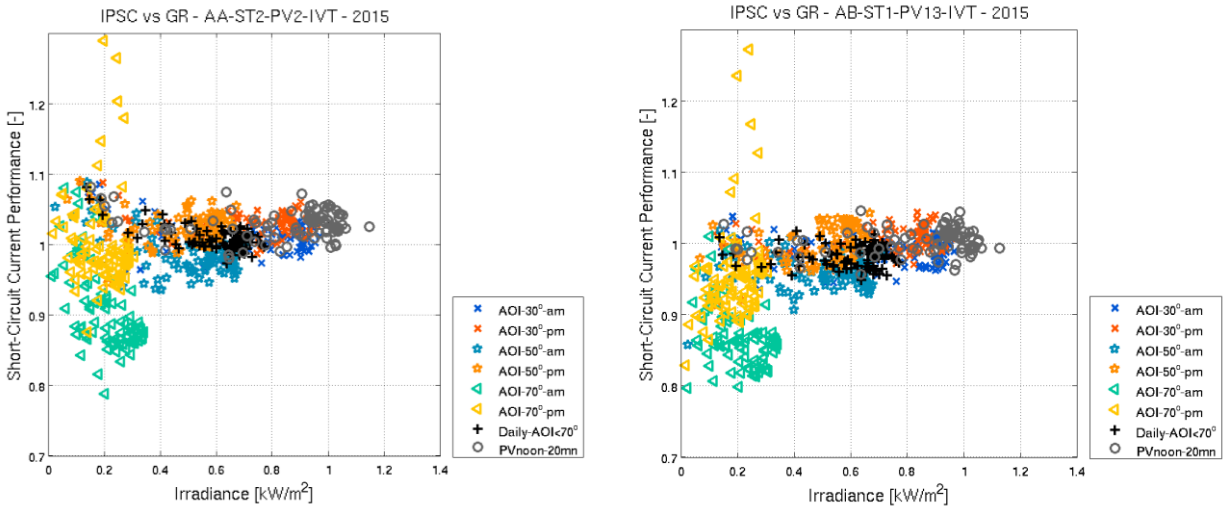

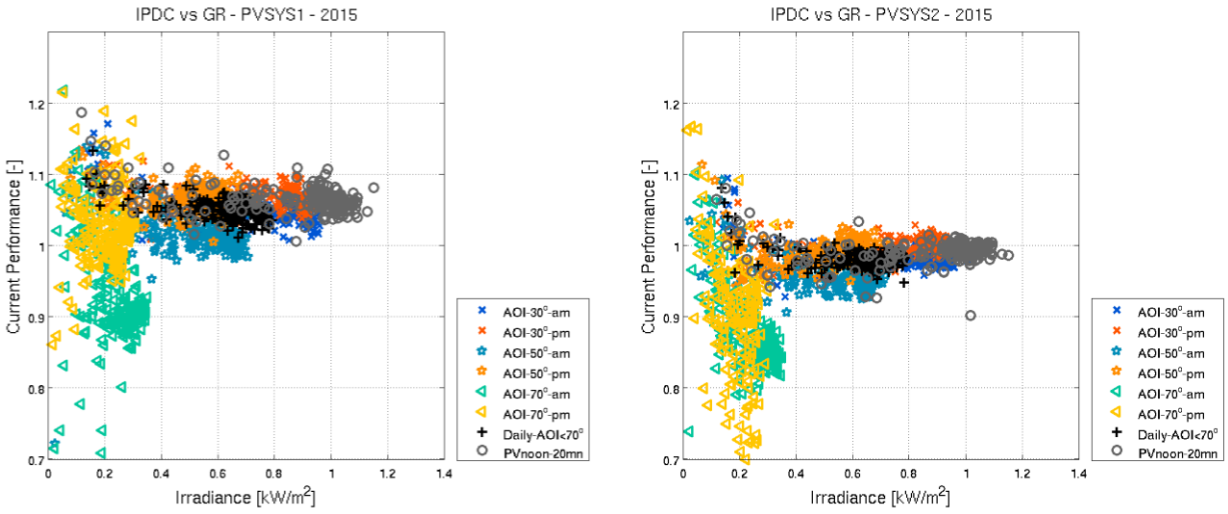

Figure 29 – IP_{SC} per AOI versus G for a-Si/µc-Si (left) and c-Si (right) modules over the second testing period (top) and PV systems (bottom).

From this analysis, we conclude that CI is an important parameter for understanding and predicting the current performance of the PV modules at our test location. This is due to the strong relationship of CI with APE, G/DB/DF, AT and AM. Plotting current performance versus CI reveals that for low CI, the performance is highly impacted by the DF component of G, which is characterized by high spectral energy leading to high performance especially for PV technologies that are sensitive to the short wavelengths. For clear sky conditions, performance decreases with decreasing G/DB, and AT when the incident radiation crosses a thicker atmospheric layer at sunrise and sunset (increasing AM). Additional analysis is necessary to further understand the IP-CI relationship observed for clear skies for daily and seasonal time scales. Observations from additional test sites would also be useful for future studies. Finally, seasonal variability is visible at peak CI, at PV noon, as we observe lower CI and higher APE in summer than in winter. Seasonal IP performance observed for the a-Si/µc-Si modules is consistent with the seasonal variation of APE. For a range of atmospheric conditions, AT may also affect the current performance. Reflection loss appears to affect PV performance at high AOI and high CI. DB is identified to have an important effect on PV performance when CI is above ~0.3. Plotting current performance versus DB demonstrates the reflection loss observed for AOI above 50° in the afternoons. IP_{SC} of the a-Si/µc-Si modules is higher than 1 indicating that compared to the standard irradiance of 1 kW/m² at AM1.5, Hawaii has high incident spectral energy. The average APE for Hawaii is estimated at 1.93eV, which is above the 1.88eV APE of the AM1.5 spectrum. APE depends strongly on location, through AM. The smaller path through the atmosphere for incident

radiation in Hawaii compared to the mainland makes Hawaii an advantageous location for PV technologies sensitive to low wavelength light. The higher IP_{SC} for a-Si/µc-Si technology demonstrates that it is a better absorber at lower G than c-Si technology, which shows little dependence on APE.

IP is determined to be an important parameter influencing the PR. In the following, the study presents the PR values for 2015. Figure 30 shows the PR versus IP for each PV system (left: a-Si/µc-Si, right: c-Si) for the year 2015. For both technologies, we observe a linear increase in PR with increasing IP. Despite noise in the datasets, these plots confirm the major impact of the current performance IP on the PR variation. We estimate that the main variation in PR is due to a variation in IP (over 30%), while we attribute only around 10% variation in PR due to a variation in the normalized voltage VN described section 3.3.

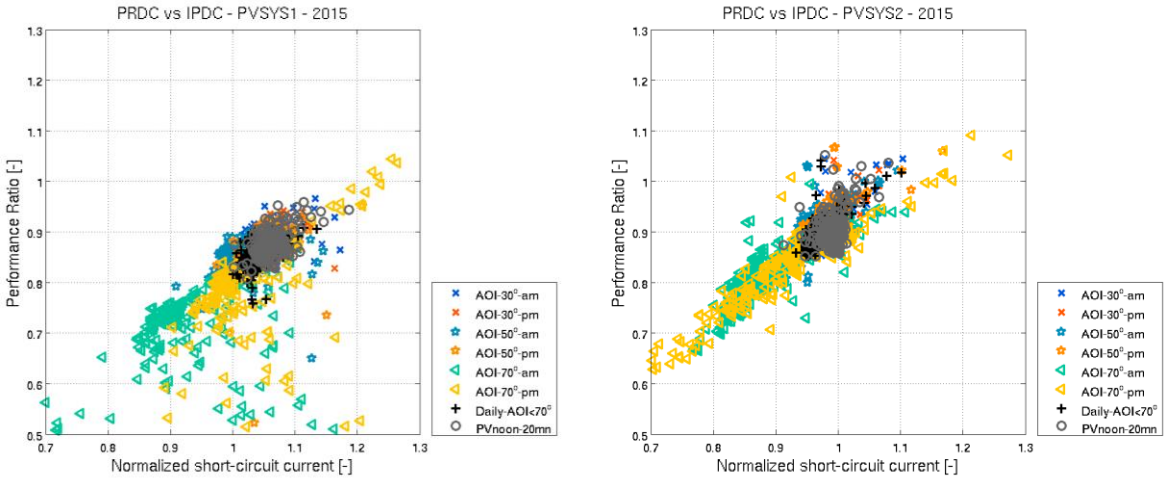

Figure 30 – PR per AOI versus IP for the PV systems (left: a-Si/µc-Si, right: c-Si) showing the current performance impact on the maximum power performance.

Figure 31 shows the monthly average variation of PR, IP and VN for the tested PV systems in 2015. We observe only small variations in PR along the year in the range of 92-94% for c-Si and 83-90% for the a-Si/µc-Si. The PR peaks in September for the a-Si/µc-Si corresponding to high IP and high VN while high PR is observed in November for the c-Si, as PR mostly varies with VN.

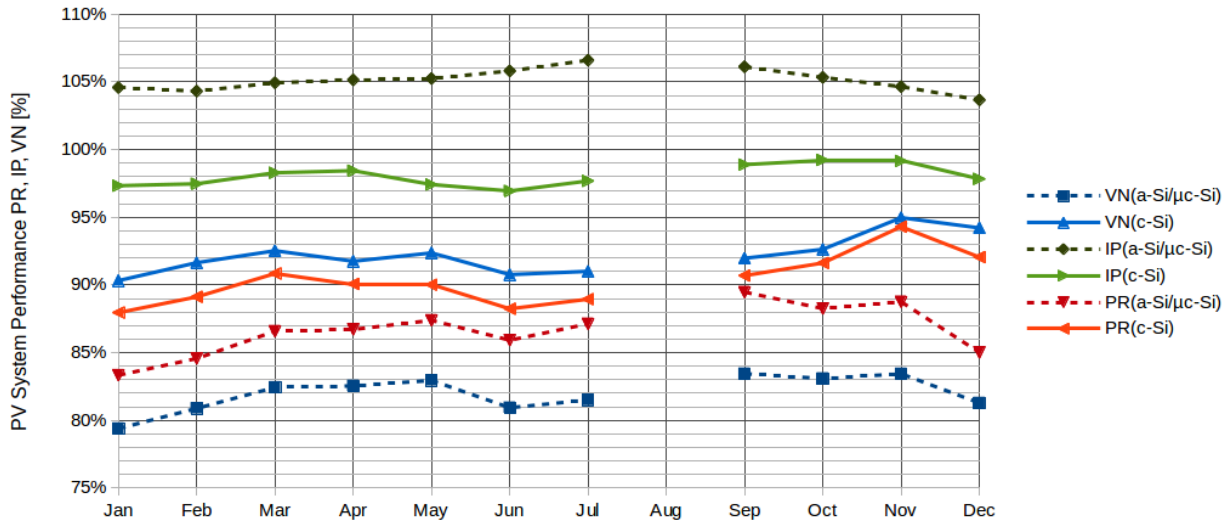

Figure 31 – Monthly PR, IP and VN versus time for both PV systems tested in 2015.

Table 3 presents the yearly average performance for each PV system and each PV module during the full period of testing. The a-Si/µc-Si PR average for 2015 is 87% while the range of PR for the individual PV modules varies between 86-90%. The c-Si PV system has an annual average PR of 91% while individual PV module PR averages are slightly higher (92-94%). As mentioned in the discussion of Figures 23 and 24, IP is higher for the a-Si/µc-Si technology (105%), representative of the average IP of the individual a-Si/µc-Si PV modules, than for the c-Si technology (98%) that is lower than the least performing individual c-Si PV modules. VN is higher for c-Si with values around 91%, whereas VN for a-Si/µc-Si reaches only 82%. For both technologies, the system VN corresponds to the maximum VN of the individual modules. More study is needed to understand the impact of individual PV module performance on to the performance of the PV system. Relative to the low VN for the a-Si/µc-Si PV modules (lower than expected by the specified temperature coefficient for the PV technology), an important degradation was estimated at 10% from observations of the voltage during the first year of operation (DE-EE0003507, U.C.A.N., 2014). This degradation results in a lower PR for the a-Si/µc-Si, around 87%, than for the c-Si, which is approximately 90%. Although we find that IP has an important influence on PR, VN also influences the PR. From this table, we observe more scatter in the performance for the a-Si/µc-Si PV modules compared to the c-Si ones.

Table 3 – Yearly average PR, IP and VN for both PV systems in 2015.

	a-Si/µc-Si		c-Si	
	PV System	PV modules	PV System	PV modules
PR	86.9%	86-90%	90.7%	92-94%
IP	105.1%	99-110%	98.2%	99-100%
VN	82.3%	73-82%	92.4%	90-92%

Finally, we conclude that IP has an important effect on daily PR variation of PV modules. Further, IP is enhanced in summer for a-Si/µc-Si, which is more the result of APE impact on IP than of AT impact. VN impacts PR values and PR variability over the year. IP is observed lower in the morning while observations of VN are lower in afternoon.

Current performance is a function of G, AT, CI, and APE. CI is shown to be an important indicator of the environmental conditions especially related to AM and to the DB/DF distribution and subsequently to the attenuation of incident irradiance. For low G, for which the main component is DF, we see an enhancement in IP due to higher APE of DF light. For low G for which the main component is DB, we see a loss in IP increasing with increasing AOI, decreasing DF, APE and AT, which is a result of recombination and reflection losses. For high G irradiance and high DB, we see a combined impact of decreasing APE and increasing AT with increasing DB/G. Hence, we conclude that increasing AT improves the current performance IP in general, while increasing APE improves the current performance of the a-Si/µc-Si technology. Our results suggest that in general, a-Si/µc-Si may be better suited to the environment and atmospheric conditions in Hawaii, as it shows less sensitivity to temperature and better absorption of the high energy incident spectrum characteristic of Hawaii. However, the a-Si/µc-Si modules suffered 1 year of degradation as evident from the voltage, thereby negatively affecting the PR values. This PV module model was actually removed from the market by the manufacturer few years after commissioning.

In addition to the PR, it is important to consider the efficiency of the PV technologies. Table 4 relates the PR to the STC efficiency, which are specified at 8.3% for a-Si/µc-Si and 13.8% for c-Si in the manufacturer's datasheet. From the PR and the STC efficiency, we determine the operational ROC efficiency to be 7.2% for a-Si/µc-Si and 12.5% for c-Si.

Table 4 – Yearly average PR, and efficiencies at STC and ROC for both PV systems in 2015.

	a-Si/µc-Si	c-Si
PR	87%	91%
STC efficiency	8.3%	13.8%
ROC efficiency	7.2%	12.6%

PR and efficiency are not the sole factors to consider when choosing a particular PV technology. For instance, the available space and cost may play a role in which module technology is chosen. The a-Si/µc-Si module requires a greater space to produce the same amount of power as a c-Si module, while, the a-Si/µc-Si module is cheaper to produce in terms of energy and material cost compared to the c-Si modules (Hordeski, 2003). In order to make an informed decision on the best technology for Hawaii, a long-term performance analysis is necessary to determine the lifetime energy production and performance.

6. Discussion

This study provides empirical results to improve our understanding of atmospheric conditions affecting PV module performance and to characterize the solar resource at the test site. The global irradiance G and its main component DB are a function of date and time, location and orientation, and cloud cover. We establish CI as an important parameter to describe atmospheric conditions and find that CI is related to the APE. The CI varies little under clear sky conditions, thus, the observed daily variation is due to cloud cover. It is under these overcast conditions that APE is observed to be elevated, indicating a spectrum shifted towards short wavelengths and increasing with increasing DF at all AOI. Further, APE decreases linearly with increasing DB at high AOI. Peak CI decreases in summer, opposite to the APE. APE increases daily as a result of cloud cover and on seasonal time scales due to lower AM in summer, particularly with increasing AOI.

Further, the study characterizes the environmental conditions for clear sky compared to overcast conditions in Hawaii. On a clear day as the sun rises with decreasing AOI, APE decreases linearly as DB increases. AT increases nearly linearly with DB. Further, DB is an important parameter to describe the intensity of irradiance. On a cloudy day, on the other hand, we observe lower DB, and lower G, lower AT, but higher APE. In summer, AM is lower, resulting in higher minimum APE values, and AT is higher.

We analyze the changes in PV module performance and efficiency, while demonstrating which parameters appear to be responsible for the observed variations in IP and PR. The comparison of the two technologies a-Si/µc-Si and c-Si for the year 2015 has shown a daily PR average of 87% and 91%, respectively. The higher PR for c-Si is largely due to a higher voltage performance. The variation in performance between tested PV modules is estimated to be higher for the a-Si/µc-Si modules than for the c-Si modules. Performance variation among modules in a system may impact PV system performance, limiting the current performance of a string of modules to the least performing module. For this study, the module wiring of the PV systems was set to six parallel strings of four PV modules for the micromorph system, which proved to be advantageous over the two parallel strings of 13 PV modules for the c-Si system. Module wiring is related to the PV technologies due to the voltage level of the PV modules (100 V_{MP} for a-Si/µc-Si and 26.6 V_{MP} for c-Si). The outdoor performance of the two PV module technologies differs also in the way that current output is affected by the environmental parameters. The PR of c-Si modules is largely impacted by temperature, with less impact from APE due to the wide spectral response of c-Si. In contrast, a-Si/µc-Si modules operate in a spectral range that is shifted towards the short-wavelength higher energy-density radiation, resulting in PR that mainly depends on the spectral irradiance distribution while being less sensitive to temperature than c-Si. These results are consistent with other studies (Minemoto et al., 2009; Cañete et al., 2014) that have shown better c-Si performance in winter while superior a-Si/µc-Si performance in summer, for which the a-Si layer is the main factor of enhancement under such conditions. Hawaii's climatic conditions are comparable to a long summer, in which a-Si/µc-Si performance is favored over much of the year. Hence, the APE dependency of a-Si/µc-Si results in higher current performance IP compared to c-Si.

As the study has shown, most environmental parameters are related, making it is challenging to isolate the impact of a single parameter. In this study, the assessment of environmental parameters has shown different impacts on the IP and PR due to the intensity, distribution, and spectrum of solar radiation. The analysis of the impact of environmental parameters on the intensity of solar irradiance suggests the following conclusions:

1. The availability of the solar resource XTR_{POA} depends on the cosine of the incident angle cos(AOI). The yearly minimum AOI is optimized at a 20° tilt for this test configuration, hence enabling the maximum energy yield.

2. DB is the main component of G, in spite of showing lower spectral energy content (as shown by APE) compared to DF.
3. The solar intensity is influenced by CI, which is impacted by cloud cover and slightly by AM.

APE proves to be a good indicator for atmospheric conditions. The range for APE for the test location is between 1.91eV and 1.96eV, which is higher than the average spectrum at AM1.5 collected on the mainland, whose energy is 1.88eV for the spectral response range of 350-1050 nm. This indicates that the solar resource at UH Manoa is characterized by generally high energy levels in terms of XTR_{POA} as well as clear sky conditions, as indicated by high CI. The analysis of the impact of environmental parameters on the solar spectrum reveals the following:

1. APE is mainly influenced by cloud cover and AM, both controlling factors of CI, whereby APE may increase with increasing cloud cover, but decreases with increasing AM.
2. At increasing AOI, seasonal variations between summer and winter become more apparent.
3. The solar spectrum is characterized by a wider range of APE at dawn/dusk due to higher DF, whereas DB, which dominates at decreasing AOI, displays a narrower range of APE values.

This paper presents the characterization of PV performance parameters and compares PV module characteristics by plotting performance characteristics (primarily IP) versus DB, CI and G. Analyzing the data as a function of DB shows the impact of APE and AT on IP. Plotting IP versus CI, we were able to distinguish several gain and loss mechanisms of the PV performance, including the daily impact of DF at low CI with high APE, as well as a seasonal impact at clear sky conditions at PV noon. Moreover, relating IP to CI shows the impact of recombination and reflection losses that vary primarily with the AOI, but also with CI and AT. Finally, although a thermal effect cannot clearly be distinguished between AT and APE or G, plotting the normalized voltage VN versus AT reveals the temperature impact on VN and thus on annual PR.

This study focuses on establishing current performance (IP) as a valid parameter to characterize PV performance. IP is a function of the irradiance G_{POA} that is largely described by DB. G and hence IP depend on the DB to DF ratio, which varies as a function of cloud cover and AOI. Thus, an informative way to study variations in IP is by plotting IP as a function of CI. When comparing both PV technologies, a-Si/µc-Si shows higher IP than the c-Si and also increased sensitivity at low G, indicating that a-Si/µc-Si are better able to absorb low wavelength light. The current performance of the a-Si/µc-Si PV

modules is enhanced by the high energy solar resource received at UH Manoa, showing better performance at peak temperatures during the day compared to c-Si. The results are influenced by the setup of the PV modules and the characteristics of the location in terms of the quality and quantity of the available solar resource. Hawaii proves to be a location with an extensive solar resource with a strong DB component and spectrum above STC, as indicated in the high APE values.

7. Conclusion and Recommendations

The solar resource received in POA depends on the available energy XTR_{POA} and cloud cover. XTR_{POA} varies largely with AOI, which depends on the PV orientation, in terms of module tilt and azimuth, and the location (latitude). For the location at UH Manoa, a high irradiation G_{POA} and high spectral energy characterize enhanced solar capabilities. Further, a low temperature variation in Hawaii limits the extent of a seasonal effect on thermal loss variation, leading to small seasonal variability in PV performance in the island environment over the course of a year (see Appendix).

This study evaluates the environmental and electrical parameters in PV operation to develop a better understanding of the performance characterization of two types of PV technologies (a-Si/µc-Si and c-Si). The irradiation received in POA at the test site in 2015 amounts to a yearly average of 5.6 kWh/m²/day, and a corresponding average CI of 0.59. DB is the main component of the irradiance, accounts for 71% of the irradiation and varies in proportion to XTR_{POA} and CI, and thus to the total irradiance G. CI is marginally impacted by AM on a daily basis due to higher absorption of light at high AOI. CI is mostly affected by cloud cover, whereby the test site results did not show a particular seasonal pattern on cloud cover. The annual average AT is 26.5°C with the highest monthly average values in September and lowest in winter. The average AM at the testing location is 1.58 for the year 2015. AM exhibits the most seasonal variation with low values in summer, e.g. AM1.31 in June, and higher AM in winter, e.g. AM2.14 in December. AM impacts all parameters to some extent, including AT, CI, APE G, DF and DB on a daily time-scale, but shows less impact on seasonal time-scales. Our results suggest that AT may explain the small seasonal variation of CI as well as the higher CI observed in the morning compared to the afternoon at this location. Finally, we concluded that APE is a very good indicator of the atmospheric conditions as it accounts for the impact of AM and cloud cover. APE varies seasonally with AM, decreasing in winter as AM increases, and is especially affected by high AOI. APE varies moreover daily with cloud cover, increasing with decreasing CI and with elevated APE values when irradiance is only diffuse.

The data analysis per AOI proved to be an effective means of visualizing the daily impact of the sun's elevation in the sky and a valid averaging method for demonstrating empirical relationships between environmental parameters and PV performance. Splitting PR into IP and VN was observed a reasonable approximation leading to easily visualize spectral enhancement on the current performance and thermal impact on the voltage. The data for PV noon, as used in this paper, is a representative part of the PV performance analysis around solar noon, characterized by a low AOI impact and indicating a particularly high DB component of irradiance under clear sky conditions. Further research may include investigating the PR at PV noon by looking at IP and VN individually, as well as in considering the most characteristic time interval over which to define PV noon. Studying clear sky performance during the full year will also lead to essential results on recombination and reflection losses in relation with seasonal change in atmospheric conditions. Additional analysis should also lead to a deeper understanding of the performance differences between short-circuit current and current at maximum power, as well as to estimate the impact of combining PV modules into a system.

The paper presents observations of local environmental conditions for ROC with a focus specifically on Hawaii. Future research may include the comparison of the impacts of environmental parameters on PV performance in different locations (particularly latitudes) of the world. The location and climatic conditions may influence the PV systems setup, including tilt and orientation, the distribution of DB to DF, and subsequently solar intensity, spectrum and energy yield. These parameters will affect the performance of various technologies differently, offering the opportunity to compare technologies operating under a range of environmental conditions.

References

Abood, A.A., 2015, A comprehensive solar angles simulation and calculation using matlab, International Journal of Energy and Environment, v. 6, p. 367–376.

Andrews, R. W., 2011, Open Source Solar Spectrum Project, Appropedia: The Sustainability Wiki. <http://www.appropedia.org/Open_source_solar_spectrum_project>.

ASTM G173-03, 2012, Standard Tables for Reference Solar Spectral Irradiances: Direct Normal and Hemispherical on 37° Tilted Surface, ASTM International, West Conshohocken, PA, doi:10.1520/G0173-03R12.

Bailey, D.A., 1999, HS440 Reading Assignment 4, University of Georgia, College of Agricultural and Environmental Sciences, 3 Aug. 1999. Web. 28 May 2016. <http://faculty.caes.uga.edu/pthomas/hort4050.web/Hort4050web/op/op4/angle.html#goback1>.

Cañete, C., Carretero, J., and Sidrach-de-Cardona, M., 2014, Energy performance of different photovoltaic module technologies under outdoor conditions, Energy, v. 65, p. 295–302, doi:0.1016/j.energy.2013.12.013.

Chen, C.J., 2011, Physics of solar energy, Print, Published by John Wiley & Sons, Inc., Hoboken, New Jersey.

Coelho, R. F., and Martins, D. C., 2012, An Optimized Maximum Power Point Tracking Method Based on PV Surface Temperature Measurement, Sustainable Energy - Recent Studies, Dr. Alemayehu Gebremedhin (Ed.), doi:10.5772/51167.

Cornaro, C., and Andreotti, A., 2012, Influence of Average Photon Energy index on solar irradiance characteristics and outdoor performance of photovoltaic modules, Progress in Photovoltaics: Research and Applications, v. 21, p. 996–1003, doi:10.1002/pip.2194.

Diffey, B., 2015, Solar Spectral Irradiance and Summary Outputs Using Excel, Photochemistry and Photobiology, v. 91, p. 553–557, doi:10.1111/php.12422.

Dubard, J., Filtz, J.-R., Cassagne, V., and Legrain, P., 2012, Solar metrology: Photovoltaic module performance measurements, XX IMEKO World Congress Metrology for Green Growth, September 9-14, 2012, Busan, Republic of Korea.

Emziane, M., and Altal, F., 2012, Orientation, air-mass and temperature effects on the optimal power output of stationary photovoltaic modules in the GCC region, International Journal of Ambient Energy, v. 33, p. 209–213, doi:10.1080/01430750.2012.711082.

Hassan, J., 2014, ARIMA and regression models for prediction of daily and monthly clearness index, Renewable Energy, v. 68, p. 421–427, doi:10.1016/j.renene.2014.02.016.

Hawaii Clean Energy Initiative, 2015, Hawaii Clean Energy Initiative, Hawaii Is the Most Fossil Fuel Dependent State in the Nation Comments. Web. <http://www.hawaiicleanenergyinitiative.org/>.

Hirata, Y., and Tani, T., 1995, Output variation of the photovoltaic modules with environmental factors. I: The effect of spectral solar radiation on photovoltaic module output, Solar Energy, v. 55, p. 463–468.

Hordeski, M.F., 2003, New Technologies for Energy Efficiency, The Fairmont Press, p. 79.

Ishii, T., Otani, K., Itagaki, A., and Utsunomiya, K., 2013, A simplified methodology for estimating solar spectral influence on photovoltaic energy yield using average photon energy, Energy Science and Engineering, v. 1, p. 18–26, doi:10.1002/ese3.3.

Keppner, H., Meier, J., Torres, P., Fischer, D., and Shah, A., 1999, Microcrystalline silicon and micromorph tandem solar cells, Applied Physics A, v. 69, p. 169–177, doi:10.1007/s003390050987.

King, D.L., 1997, Photovoltaic module and array performance characterization methods for all system operating conditions, Proceeding of NREL/SNL Photovoltaics Program Review Meeting, November 18-22,1996, Lakewood, CO, AIP Press, New York, 1997.

King, D.L., Boyson, W.E., and Kratochvil, J.A., 2004, Photovoltaic array performance model. Report SAND2004-3535. <http://www.sandia.gov/pv/docs/PDF/King%20SAND.pdf>.

Kurtz, S., Whitfield, K., Miller, D., Joyce, J., Wohlgemuth, J., Kempe, M, Dhere, N., Bosco, N., and Zgonena, T., 2009, Evaulation of high-temperature exposure of photovoltaic modules, Conference Paper NREL/CP-520-45986.

Kyocera Datasheet, Model KD205GX-LP.

Litjens, G., 2013, Investigation of spectral effects on photovoltaic technologies by modelling the solar spectral distribution, University Utrecht, Faculty of Geosciences Theses, Master Thesis in Energy Science.

Mitsubishi Heavy Industries Datasheet, Model MT130.

Merten, J., and Andreu, J., 1998, Clear separation of seasonal effects on the performance of amorphous silicon solar modules by outdoor I/V-measurements, Solar Energy Materials and Solar Cells, v.52, p. 11–25, doi;10.1016/S0927-0248(97)00263-8.

Moreno, J.C., Serrano, M.A., Cañada, J., Gurrea G., Utrillas, M.P., and Solar Radiation Group, 2014, Effect of the relative optical air mass and the clearness index on solar erythemal UV irradiance, Journal

of Photochemistry and Photobiology B: Biology, v. 138, p. 92–98, doi:10.1016/j.jphotobiol.2014.05.005.

Minemoto, T., Nakada, Y., Takahashi, H., and Takakura, H., 2009, Uniqueness verification of solar spectrum index of average photon energy for evaluating outdoor performance of photovoltaic modules, Solar Energy, v. 83, p. 1294–1299, doi:10.1016/j.solener.2009.03.004.

Minemoto, T., Yamasaki, K., and Takakura, H., 2011, Relationship of spectral irradiance distribution and average photon energy for analyzing the impact of solar spectrum on photovoltaic module performance, 26th European Photovoltaic Solar Energy Conference, p. 3345–3348.

Moreno-Sáez, R., Sidrach-de Cardona, M., and Mora-López, L., 2013, Characterization of solar spectral irradiance using the index of average photon energy for its use in the performance evaluation of PV modules, 28th European Photovoltaic Solar Energy Conference and Exhibition, WIP Munich, p. 3200–3202.

Moreno-Sáez, R., Sidrach-de-Cardona, M., and Mora-López, L., 2016, Analysis and characterization of photovoltaic modules of three different thin-film technologies in outdoor conditions, Applied Energy, v. 162, p.827-838, doi:10.1016/j.apenergy.2015.10.156.

Nakada, Y., Takahashi, H., Ichida, K., Minemoto, T., and Takakura, H., 2010, Influence of clearness index and air mass on sunlight and outdoor performance of photovoltaic modules, Current Applied Physics, v. 10, pp. 261–264, doi:10.1016/j.cap.2009.11.026.

National Renewable Energy Laboratory Martin Rymes, 2000, “Solar Position and Intensity 2.0”. <http://rredc.nrel.gov/solar/codesandalgorithms/solpos/aboutsolpos.html#refs>.

Nordmann, T, Clavadetscher, L., van Sark, W.G.J.H.M., and Green, M., 2014, Analysis of Long-Term Performance of PV Systems, IEA International Energy Agency Photovoltaic Power Systems Programme, Report IEA-PVPS T13-05:2014, ISBN 978-3-906042-21-3.

Norton, M., Gracia Amillo, A.M., and Galleano R., 2015, Comparison of solar spectral irradiance measurements using the average photon energy parameter, Solar Energy, v. 120, p. 337–344, doi:10.1016/j.solener.2015.06.023.

Okada, N., Yamanaka, S., Kawamura, H., Ohno, H., and Kawamura, H., 2003, Energy loss of photovoltaic system caused by irradiance and incident angle, 3rd World Conference on Photovoltaic Energy Conversion, v. 2, pp. 2062–2065.

Ormachea, O., Abrahamse, A., Tolavi, N., Romero, F., Urquidi, O., Pearce, J. M., and Andrews R., 2013, Installation of a variable-angle spectrometer system for monitoring diffuse and global solar radiation,

Proceedings of SPIE, v. 8785, 8th Iberoamerican Optics Meeting and 11th Latin American Meeting on Optics, Lasers, and Applications, doi:10.1117/12.2025480.

Parretta, A., Sarno, A., and Vicari, L.R.M., 1998, Effects of solar irradiation conditions on the outdoor performance of photovoltaic modules, Optics Communications, v. 153, p. 153–163, doi:10.1016/S0030-4018(98)00192-8.

Pierro, M., Bucci, F., and Cornaro, C., 2014, Full characterization of photovoltaic modules in real operating conditions: theoretical model, measurement method and results, Progress in Photovoltaics: Research and Applications, v. 23, p. 443–461, doi:10.1002/pip.

Reynolds, S., and Smirnov, V., 2015, Modelling performance of two- and four-terminal thin-film silicon tandem solar cells under varying spectral conditions, Energy Procedia, v. 84, p. 251–260, E-MRS Spring Meeting 2015 Symposium C - Advanced inorganic materials and structures for photovoltaics, doi: 10.1016/j.egypro.2015.12.321.

Roumpakias, E., Zogou, O., and Stamatelos A., 2015, Correlation of actual efficiency of photovoltaic panels with air mass, Renewable energy, v. 74, p. 70–77, doi:10.1016/j.renene.2014.07.051.

Sandia National Laboratories, 2014, Extraterrestrial Radiation, PV Performance Modelling Collaborative, Web. <https://pvpmc.sandia.gov/modeling-steps/1-weather-design-inputs/irradiance-and-insolation-2/extraterrestrial-radiation/>.

Schimmrich, S., 2011, Vernal Equinox, Hudson Valley Geologist. N.p., 20 Mar. 2011. Web. 28 May 2016. <http://hudsonvalleygeologist.blogspot.com/2011_03_01_archive.html>.

Silverman, T.J., Jahn, U., Friesen, G., Pravettoni, M., Apolloni, M., Louwen, A., van Sark, W.G.J.H.M., Schweiger, M., Belluardo, G., Wagner, J. and Tetzlaff, A., 2014, Characterisation of Performance of Thin-film Photovoltaic Technologies, IEA International Energy Agency Photovoltaic Power Systems Programme, Report IEA-PVPS T13-02:2014, ISBN 978-3-906042-17-6.

Sirisamphanwong, C., Ketjoy, N., and Sirisamphanwong, C., The effect of average photon energy and module temperature on performance of photovoltaic module under Thailand's climate condition, 2014, Energy Procedia, v. 56, p. 359–366, 11th Eco-Energy and Materials Science and Engineering (11th EMSES), doi:10.1016/j.egypro.2014.07.168.

Sirisamphanwong, C., Ketjoy, N., Rakwichain, W., Vaivudh, S., 2011, Average photon energy under Thailand's climatic condition, International Journal of Renewable Energy, v. 6.

Skoplaki, E., and Palyvos, J.A., 2009, On the temperature dependence of photovoltaic module electrical performance: A review of efficiency/power correlations, Solar Energy, v. 83, p. 614–624, doi:10.1016/j.solener.2008.10.008.

Solar Energy Industries Association, 2015, 2014 Top 10 Solar States, Solar Energy Industries Association (SEIA), Web. <http://www.seia.org/research-resources/2014-top-10-solar-states>.

Stein, J.S., Sutterlueti, J., Ransome, S., Hansen, C.W., and King, B. H., 2013, Outdoor PV performance evaluation of three different models: Single-diode, SAPM and Loss Factor Model, in: 28th European PV Solar Energy Conference, Paris, France, 2013.

Touati, F., Al-Hitmi, M.A. Chowdhury, N.A. Hamad, J.A., and San Pedro Gonzales, A.J.R., 2016, Investigation of solar PV performance under Doha weather using a customized measurement and monitoring system, Renewable Energy, v. 89, p. 564–577, doi:10.1016/j.renene.2015.12.046.

DE-EE0003507, U.C.A.N., 2014, Performance and Analysis of Different Photovoltaic Technologies at Selected Sites.

van Dam, B., 2013, Accounting for variations in the spectral irradiance distribution in pv panel performance model, University Utrecht, Faculty of Geosciences Theses, Master Thesis in Energy Science.

Williams, S.R., Betts, T.R., Helf, T., Gottschalg, R., Beyer, H.G., and Infield, D.G., 2003, Modelling long-term module performance based on realistic reporting conditions with consideration to spectral effects, 3rd World Conference on Photovoltaic Energy Conversion, v. 2, pp. 1908–1911.

Williams, S.R., Gottschalg, R., and Infield, D.G., 2003, Performance of photovoltaic modules in a temperate maritime climate, 3rd World Conference on Photovoltaic Energy Conversion, v. 2, pp. 2070–2073.

Wilson, A., and Ross, R., 1983, Angle-of-incidence effects on module power and energy performance, Progress Report 21 and Proceedings of the 21st Project Integration Meeting, Jet Propulsion Laboratory, Pasadena, CA, 1983, pp. 423-426.

Zdanowicz, T., Rodziewicz, T., and Waclawek, M.Z., 2003, Effect of air mass factor on the performance of different type of PV modules, 3rd World Conference on Photovoltaic Energy Conversion, v. 2, pp. 2019–2022.

Appendix

i. Datasheet for MHI (a-Si/µc-Si)) PV modules.

ii. Datasheet for KYO (c-Si) PV modules.

iii. Monthly and yearly results for electrical performance.

i. Datasheet for MHI (a-Si/µc-Si) PV modules.

Mitsubishi Tandem Photovoltaic Module

After more than five years of producing reliable and extremely high-quality amorphous silicon photovoltaic modules, MHI has successfully developed and commercialized a new generation of micromorph tandem-type modules with even higher generating capacities.

These tandem modules have a double-layer structure with a microcrystalline silicon film on an amorphous silicon film. The solar absorption spectrum of these modules extends from ultraviolet to visible and infrared wavelengths, assuring the generation of considerably more power than can be expected from the conventional amorphous modules from MHI. The thin-film structure enables the manufacture of the modules with only small amounts of silicon and energy, extending the reduction of CO_2 emissions over conventional crystalline modules.

The next generation of tandem photovoltaic modules from MHI expand the possibilities of clean energy by combining high efficiency with environmental care.

Comparison of power production (ISET*)

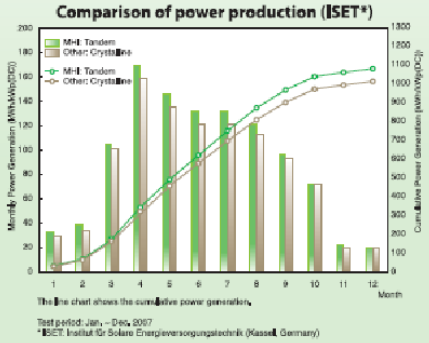

The line chart shows the cumulative power generation.

Test period: Jan. – Dec. 2007
* ISET: Institut für Solare Energieversorgungstechnik (Kassel, Germany)

SPECIFICATIONS

Mechanical Characteristics

Model	MT130
Dimensions (Length x Width x Thickness)	1,414 mm x 1,114 mm x 35 mm
Weight	Approx. 21 kg

Electrical Characteristics

Maximum power	130 W
Maximum power voltage	100 V
Maximum power current	1.30 A
Open circuit voltage	130 V
Short circuit current	1.59 A
Maximum system voltage	600 V

Temperature Coefficients

Maximum power (W)	-0.28%/°C
Maximum power voltage (V)	-0.33%/°C
Maximum power current (A)	+0.06%/°C
Open circuit voltage (V)	-0.32%/°C
Short circuit current (A)	+0.06%/°C

Measurements made under the standard test conditions (STC):
- Irradiance of 1 kW/m²
- Spectrum of AM1.5
- Module temperature of 25°C

* MHI reserves its rights to change without prior notice the contents of this data.

Appearance

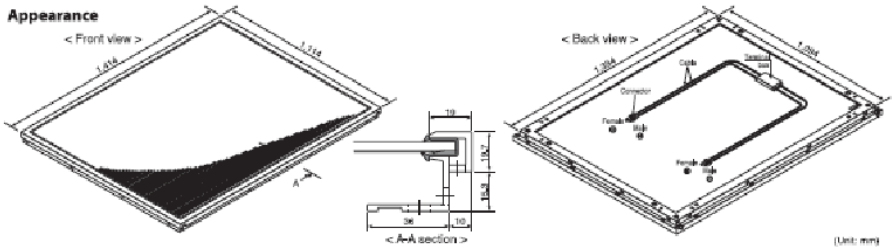

I-V curve in various temperature

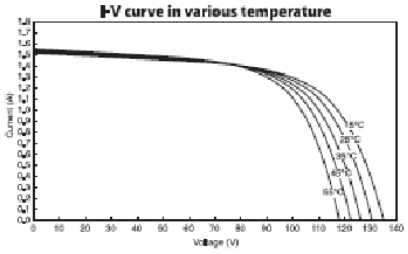

I-V curve in various irradiance

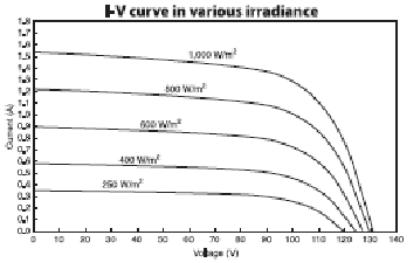

Wiring Principle

Mitsubishi Tandem PV modules connection functional system reduces the need of special cables and connection box, and thus substantially contributes to cost reduction.

(a) Parallel connection
PV modules can be connected in parallel by fastening together adjacent positive cables, and together adjacent negative cables.

(b) Series connection
PV modules can be connected in series by fastening the positive cable of one parallel string and the negative cable of another parallel string.

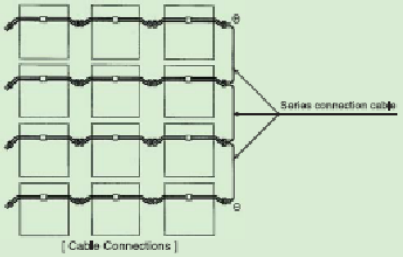

[Cable Connections]

MITSUBISHI HEAVY INDUSTRIES, LTD.

Renewable Energy Business Division
Solar Power System Business Unit
3-1, Minatomirai 3-chome, Nishi-ku, Yokohama 220-8401, Japan
Tel: +81-45-200-7922 Fax: +81-45-200-7738
E-mail for contact: photovoltaic@mhi.co.jp URL: http://www.mhi.co.jp/power/e_a-si

Printed in Japan

ii. Datasheet for KYO (c-Si) PV modules.

THE NEW VALUE FRONTIER

KYOCERA

KD205GX-LP

HIGH EFFICIENCY MULTICRYSTAL
PHOTOVOLTAIC MODULE

LISTED

HIGHLIGHTS OF KYOCERA PHOTOVOLTAIC MODULES

Kyocera's advanced cell processing technology and automated production facilities produce a highly efficient multicrystal photovoltaic module.
The conversion efficiency of the Kyocera solar cell is over 16%.
These cells are encapsulated between a tempered glass cover and a pottant with back sheet to provide efficient protection from the severest environmental conditions.
The entire laminate is installed in an anodized aluminum frame to provide structural strength and ease of installation.
Equipped with plug-in connectors.

APPLICATIONS

KD205GX-LP is ideal for grid tie system applications.

- Residential roof top systems
- Large commercial grid tie systems
- Water Pumping systems
- High Voltage stand alone systems
- etc.

QUALIFICATIONS

- **MODULE** : UL1703 listed
- **FACTORY** : ISO9001 and ISO 14001

ELECTRICAL CHARACTERISTICS

Current-Voltage characteristics of Photovoltaic Module KD205GX-LP at various cell temperatures

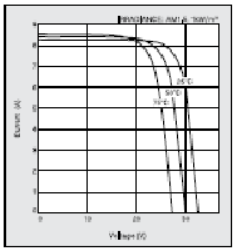

Current-Voltage characteristics of Photovoltaic Module KD205GX-LP at various irradiance levels

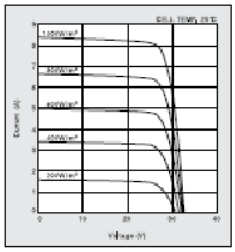

0503

Specifications

Electrical Performance under Standard Test Conditions (*STC)	
Maximum Power (Pmax)	205W (+5%/−5%)
Maximum Power Voltage (Vmpp)	26.6V
Maximum Power Current (Impp)	7.71A
Open Circuit Voltage (Voc)	33.2V
Short Circuit Current (Isc)	8.36A
Max System Voltage	600V
Temperature Coefficient of Voc	−0.120 V/°C
Temperature Coefficient of Isc	5.02×10^{-3} A/°C

*STC : Irradiance 1000W/m², AM1.5 spectrum, cell temperature 25°C

Electrical Performance at 800W/m², *NOCT, AM1.5	
Maximum Power (Pmax)	145W
Maximum Power Voltage (Vmpp)	23.5V
Maximum Power Current (Impp)	6.17A
Open Circuit Voltage (Voc)	29.9V
Short Circuit Current (Isc)	6.82A

*NOCT (Nominal Operating Cell Temperature): 45°C

Cells	
Number per Module	54

Module Characteristics	
Length × Width × Depth	1500mm(59.1in)×990mm(39.1in)×46mm(1.8in)
Weight	18.5kg(40.8lbs.)
Cable	(+)760mm(29.9in),(-)1041mm(41.0in)

Junction Box Characteristics	
Length × Width × Depth	100mm(3.9in)×106mm(4.3in)×15mm(0.6in)
IP Code	IP65

Others	
*Operating Temperature	−40°C ~ +90°C
Maximum Fuse	15A

*This temperature is based on cell temperature.

iii. Daily variation of electrical performance characteristics of the two PV systems operating at GHHI for the year 2015.

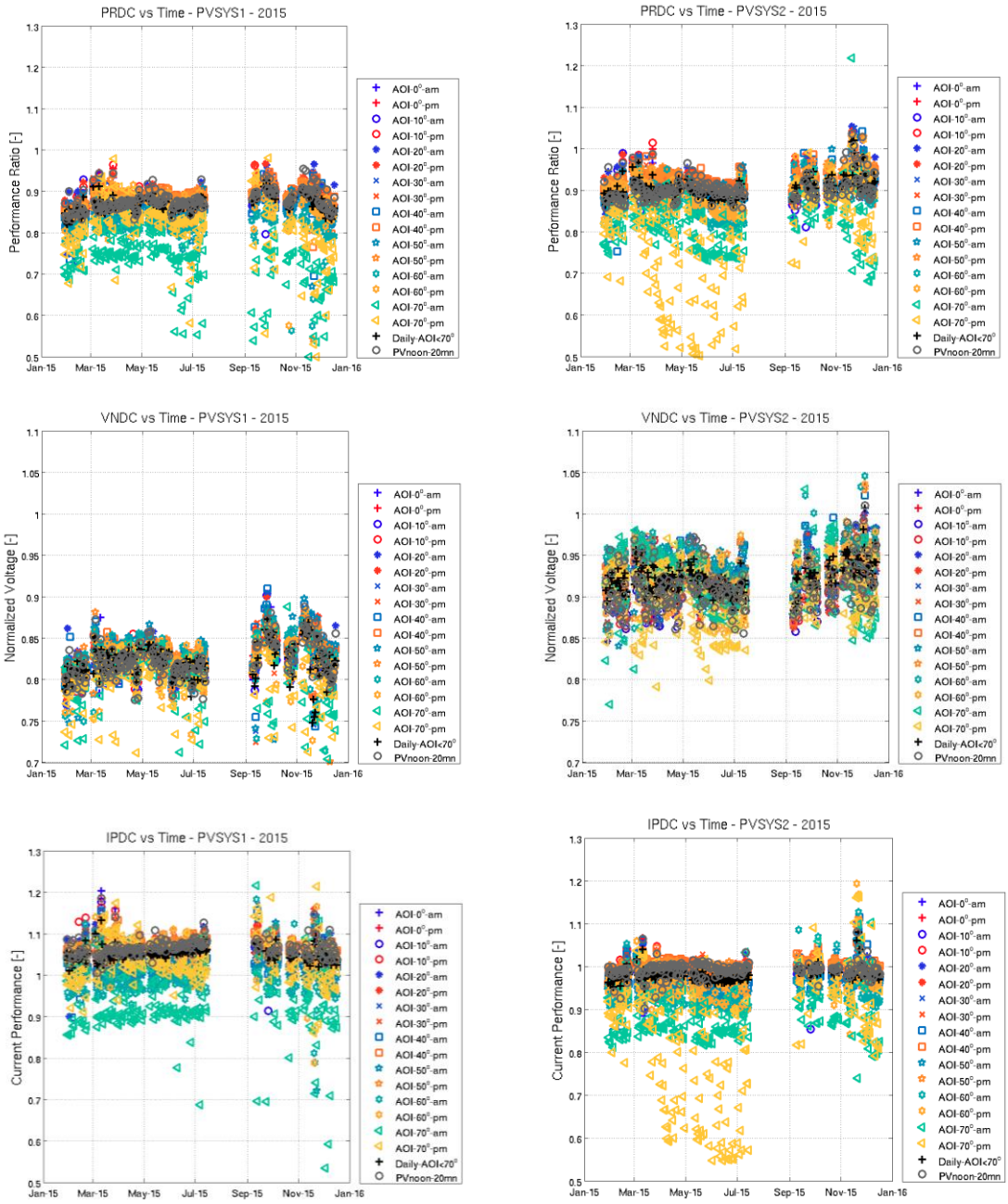

Figure 32 – PR, VN and IP of the a-Si/µc-Si (left) and c-Si (right) PV systems (2015) for all AOI. Lower VN in summer (following temperature) - higher AOI impact on VN (lower in the afternoon, negative temperature coefficient). PR combine with impact on IP (lower during summer for a-Si/µc-Si favored by sensitivity to APE (bluer wavelength) and lower temperature impact on VN.